inorganics

MDPI

Review

Solvothermal Synthesis Routes to Substituted Cerium Dioxide Materials

James W. Annis [1], Janet M. Fisher [2], David Thompsett [2] and Richard I. Walton [1,*]

[1] Department of Chemistry, University of Warwick, Coventry CV4 7AL, UK; J.Annis@warwick.ac.uk
[2] Johnson Matthey Technology Centre, Sonning Common, Reading RG4 9NH, UK; janet.fisher@matthey.com (J.M.F.); thompd@matthey.com (D.T.)
* Correspondence: r.i.walton@warwick.ac.uk

Abstract: We review the solution-based synthesis routes to cerium oxide materials where one or more elements are included in place of a proportion of the cerium, i.e., substitution of cerium is performed. The focus is on the solvothermal method, where reagents are heated above the boiling point of the solvent to induce crystallisation directly from the solution. This yields unusual compositions with crystal morphology often on the nanoscale. Chemical elements from all parts of the periodic table are considered, from transition metals to main group elements and the rare earths, including isovalent and aliovalent cations, and surveyed using the literature published in the past ten years. We illustrate the versatility of this synthesis method to allow the formation of functional materials with applications in contemporary applications such as heterogeneous catalysis, electrodes for solid oxide fuel cells, photocatalysis, luminescence and biomedicine. We pick out emerging trends towards control of crystal habit by use of non-aqueous solvents and solution additives and identify challenges still remaining, including in detailed structural characterisation, the understanding of crystallisation mechanisms and the scale-up of synthesis.

Keywords: ceria; hydrothermal; catalysis; nanomaterials; crystallisation

Citation: Annis, J.W.; Fisher, J.M.; Thompsett, D.; Walton, R.I. Solvothermal Synthesis Routes to Substituted Cerium Dioxide Materials. *Inorganics* **2021**, *9*, 40. https://doi.org/10.3390/inorganics9060040

Academic Editor: Duncan H. Gregory

Received: 22 April 2021
Accepted: 11 May 2021
Published: 21 May 2021

1. Introduction

Cerium dioxide, ceria, is well known for significant applications in heterogeneous catalysis, where it is frequently used as a redox-active support [1,2]. This chemistry is exploited in numerous practical applications, exemplified by its use as the oxygen storage component in three-way catalytic convertors, as a support for precious metals for destruction of CO, NO_x and hydrocarbon emissions in automotive exhausts [3–5]. There are many emerging applications of ceria in catalysis and these include use in steam reforming [6], soot oxidation [7], water–gas shift [8], oxidation of volatile organics [9] and thermochemical water splitting [10]. All of these rely on the ease of reversible release of oxygen from the solid that has the cubic fluorite structure type, which is well known for its oxide ion migration properties, accompanied by the reversible reduction of Ce^{4+} to Ce^{3+}.

Another important developing application of ceria is as an oxide-conducting electrolyte in solid oxide fuel cells [11]. Ceria-based solid electrolytes show promising conductivity in the temperature range 500–700 °C, and here, oxide ion vacancies are vital to optimise the hopping of ions to carry charge. Beyond heterogeneous catalysis and ionic conductors, biomedical applications of ceria are under development, such as in antioxidant defense [12–14]. The material also finds use in UV shielding [15–17], as an abrasive agent [18] and in humidity sensors [19].

For most real samples of ceria, the ideal formula CeO_2 is not found: in reality, there are typically some levels of oxide defects and hence the presence of Ce^{3+} to give the formula $CeO_{2-\delta}$ [20]. These intrinsic defects are inherently beneficial for the oxide ion migration that gives rise to many of the materials' useful properties, since bulk oxygen mobility is enhanced, but in order to further enhance defects, partial substitution of Ce by a second cation, *M*, to

give ternary materials $Ce_{1-x}M_xO_{2-\delta}$ is a common strategy. (Note that in this article, we refer to this replacement as substitution to indicate that a proportion of cerium is swapped for a second cation, rather than "doping", which implies the addition of a second species.) If *M* is aliovalent (a trivalent cation or divalent cation), then a greater proportion of oxide ion vacancies are needed to balance the charge, Figure 1. However, even replacement of Ce by an isovalent cation (such as Zr^{4+} or Hf^{4+}) engenders useful properties: the local distortion of the structure due to the size mismatch of the ions introduces high lattice strain [5]. This makes these solid solutions highly reducible with a significant proportion of the bulk cerium being reduced at moderate temperatures, with redox properties maintained over many cycles of reduction–oxidation. Hence, ceria-zirconia has become one of the most widely studied materials for redox catalysis, especially as a support for precious metals [21].

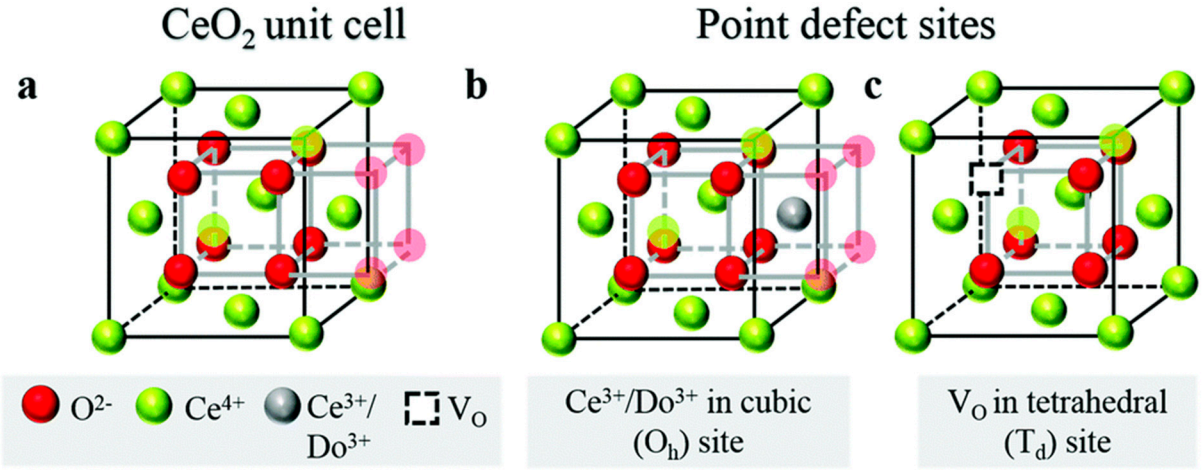

Figure 1. Schematic of crystal structure and defects for ceria and substituted variant [20]. (**a**) The fluorite ceria unit cell, containing 8 oxygen atoms (red) forming a simple cube embedded inside a face-centred cubic (FCC) array of Ce cations (green). Every second oxygen cube contains a Ce cation, as illustrated by the 4 semi-transparent oxygen atoms on the right, belonging to the next unit cell. Overall, the fluorite unit cell has 8 oxygen atoms and 4 cerium atoms. (**b**,**c**) Illustration of the two main point defects which may or may not be preferentially nearest neighbours, depending on the dopant type and prevalence of oxygen deficiency. Cation defects, Ce^{3+} (in oxygen-deficient ceria) and Do^{3+} (in substituted ceria), sit in a Ce^{4+} cubic site of Oh symmetry with 8-fold oxygen coordination. Every two cation defects in the structure are balanced by one oxygen vacancy defect, V_O, which sits in a tetrahedral site of Td symmetry, with 4-fold cation coordination. Reproduced from Schmitt, R.; Nenning, A.; Kraynis, O.; Korobko, R.; Frenkel, A.I.; Lubomirsky, I.; Haile, S.M.; Rupp, J.L.M. A review of defect structure and chemistry in ceria and its solid solutions. *Chem. Soc. Rev.* **2020**, *49*, 554–592, published by The Royal Society of Chemistry [20].

Coupled with substitutional chemistry is the effect of texture and crystal morphology on the properties of cerium oxide materials. For catalysis, the high surface area offered by small crystallites is desirable, but the shape and crystal habit can also affect properties, and for ceria, this includes the redox associated with oxygen loss and gain. Thus, the activity of ceria in catalysis may depend crucially on crystal habit, particularly when nanoscale crystallites are considered [22–26], and when the material is used as a support for precious metals, when specific crystal faces may offer favourable interactions. Similar relationships have been found for ceria-zirconia solid solutions [27,28].

In general, there is a need to develop reproducible methods for control of the synthesis of nanostructured ceria materials [29], and this article will review the recent literature that deals with the solvothermal synthesis of substituted cerium dioxide materials. We will focus on the literature from the past decade, since 2010, and for the previous literature, we direct the reader to a previous review article that considered the earlier literature on solvothermal crystallisation of various oxides of cerium [30].

2. Solvothermal Synthesis of Oxides

The term hydrothermal refers to the use of water as a reaction medium when heated at or above its boiling point in a closed vessel, where autogeneous pressure is introduced [31,32]. The method has been explored since the 1840s as a means of preparation of analogues of naturally found minerals, is well known for the synthesis of zeolites and as such has been intensely developed since the 1940s [33]. Preparative hydrothermal synthesis was also developed for the growth of large crystals of dense materials, such as quartz [34]. The term solvothermal was later introduced by Demazeau to encompass the use of any solvent heated above its boiling point [35]. In terms of the synthesis of oxides, solvothermal synthesis methods (in fact, commonly hydrothermal) have been applied for a variety of materials from binary phases to more complex multinary compositions. Here, the emphasis is often on the use of rather mild conditions (typically around 200 °C, where 10 s of bar pressure may be developed) for the formation of fine powders of a material [36–40]. Earlier review articles described the changes in water properties that occur when it is heated in sealed vessels, and these may include changes in viscosity and dielectric constant such that otherwise insoluble reagents are solubilised and dissolution–recrystallisation may take place [31,32]. Often, a mineraliser is added to the crystallisation, whose role is to aid the dissolution of reagents, and commonly alkali-metal hydroxides or fluorides are used.

The advantage of solvothermal synthesis over other methods is that crystallisation of the desired phase occurs directly from the solution, offering the potential for control of crystal habit directly at the point of synthesis, without any high temperature annealing necessary to induce crystallisation and that might destroy any intricate crystal form. We will thus focus one such one-step synthesis, without annealing or firing to bring about crystallisation. Commonly, however, calcination up to 500 °C is employed to remove any excess solvent before study, particularly when catalytic properties are to be investigated, but this is a considerably lower temperature method than employed in other methods, such as precipitation firing, combustion or thermal decomposition of precursor salts. Interestingly, early work on ceria synthesis in the 1980s used extreme hydrothermal conditions (up to 700 °C and 100 MPa) with the aim of growth of large crystals (100 μm in dimension) [41], but the focus since then has almost entirely been on the formation of fine powders, particularly with nanostructure. Under these milder conditions, synthesis is conveniently carried out in the laboratory using Teflon™-lined steel reactors.

3. Survey of Substituted Cerium Oxides

3.1. Ceria-Zirconia

As noted above, the replacement of Ce^{4+} by isovalent Zr^{4+} is one the most widely studied substitutions used to tune the properties of ceria. In fact, this gives a complete substitutional series, $Ce_{1-x}Zr_xO_2$, from cubic cerium-rich compositions with $x < 0.1$, to tetragonal zirconium-rich phases with $x > 0.1$, and monoclinic for the most zirconia-rich materials, $x > 0.88$ [2]. Note that these are equilibrium crystal structures for materials prepared at high temperature, and the degree of tetragonality may be small for $x < 0.5$ and can also be difficult to detect when a diffraction profile is broadened due to the small crystal domain size, giving rise to pseudo-cubic materials. There is also the possibility of various metastable phases that depend on the composition and preparative method, and coupled with the possibility of atomic-scale inhomogeneity and nanoscale phase segregation, this makes determination of the precise structure of ceria-zirconia solid solutions challenging [42]. Even in the pseudo-cubic materials, the smaller ionic radius of zirconium compared to cerium induces local distortion of the structure, which is believed to be responsible for the enhanced oxygen storage capacity and more favourable reducibility, and this is also accompanied by enhanced thermal stability [5]. The precise redox and other catalytic properties depend on composition and which crystal phase is present, and here, the low temperatures of solvothermal synthesis offer the possibility of control over polymorphism, or the formation of mixed-phase samples with desirable properties. For example, Yang et al. used a solvothermal synthesis method from a mixed

solvent of ethanol, *N*,*N*-dimethylformamide and ethylene glycol in the presence of lauric acid to form a ceria-zirconia with a Ce/Zr molar ratio of ~7/3; even in this ceria-rich composition, a mixed cubic (41%) and tetragonal (59%) sample was formed with distinct cubic–tetragonal interfaces on the nanoscale, Figure 2 [43]. Typically, to engineer such interfaces, high-temperature treatment above 1000 °C is needed to induce phase separation, and the advantage of the solvothermal approach is the high surface areas of the materials, which Yang et al. showed offered good activity for soot oxidation, ascribed to the presence of cubic–tetragonal interfaces, which significantly enhance the formation of oxygen vacancies from release of surface lattice oxygen.

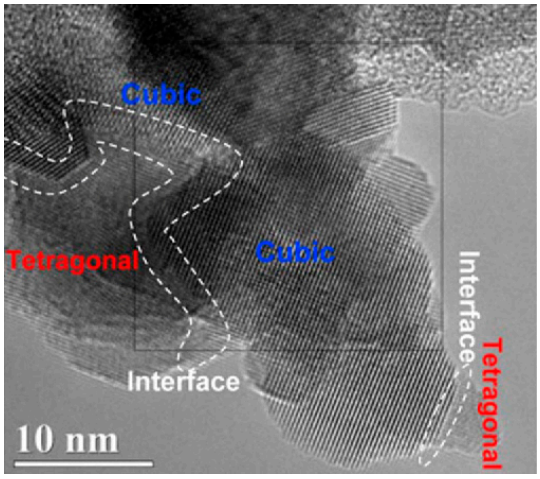

Figure 2. Cubic–tetragonal interfaces in ceria-zirconia prepared by a mixed-solvent solvothermal synthesis [43]. Reprinted from Yang, Z.; Hu, W.; Zhang, N.; Li, Y.; Liao, Y. Facile synthesis of ceria–zirconia solid solutions with cubic–tetragonal interfaces and their enhanced catalytic performance in diesel soot oxidation. *J. Catal.* **2019**, *377*, 98–109, with permission from Elsevier.

In general, solvothermal synthesis allows surface properties of ceria materials to be modified, compared to materials prepared by conventional methods. Luciani et al. prepared $Ce_{0.75}Zr_{0.25}O_2$ by two hydrothermal routes, one with 1-propanol as a co-solvent and the other with urea as an additive, and X-ray photoelectron and electron paramagnetic resonance spectroscopies showed an increase in both surface and bulk Ce^{3+} content, corresponding to a higher oxygen mobility [44]. Wang et al. also used urea-assisted hydrothermal synthesis to prepare defect-rich ceria-zirconia materials, with the highest levels of defects seen for the zirconia-rich phases, and used these materials as catalysts for the oxidative dehydrogenation of ethylbenzene with CO_2 [45].

The benefits of solvothermal synthesis in controlling crystal morphology have been explored for ceria-zirconia materials, and Table 1 summarises some of the key examples. These illustrate how the crystal shape on the nanoscale can be adjusted from isotropic to anisotropic plates and rods by choice of reagents and solvent. Figure 3 shows an example of how morphology can be selected from facetted polyhedral to rod-shaped and plate-like with the crystal dimension on the nanoscale by choice of reagents, solution additives and temperature (and/or time of reaction) [46].

An orientated attachment mechanism was proposed by Liu et al., who formed hollow, truncated octahedral agglomerates of primary particles of cerium-rich compositions [47]. However, in general, the crystallisation mechanism and the origin of the shape control that is possible by synthesis have not been determined. Clearly, this is an area where further work is needed. Some observations have been made on the relationship between crystal morphology and the resulting properties. For example, CeO_2 nanorods were shown to have higher activity towards CO oxidation than CeO_2 nanoparticles, primarily because of the preferential exposure of the reactive {110} planes, but ZrO_2 doping promoted the reducibility of the nanoparticles more significantly than that of the nanorods [48].

Table 1. Summary of solvothermal conditions used to prepare various crystal morphologies of $Ce_xZr_{1-x}O_2$.

Crystal Morphology	Composition $Ce_xZr_{1-x}O_2$	Solvent Temperature Time [a]	Reagents	Reference
Facetted polyhedral 3–5 nm diameter	$0 \leq x \leq 1$	6 M NaOH(aq) 150 °C 48 h	$Ce(NO_3)_3 \cdot 6H_2O$ $ZrO(NO_3)_2 \cdot xH_2O$	[49]
Hollow, truncated octahedral ~80 nm edge	x = 0.01, 0.1, 0.2	water 100 °C 18 h	$CeCl_3 \cdot 7H_2O$ $ZrOCl_2 \cdot 8H_2O$ Poly(vinylpyrrolidone) H_2O_2 formic acid tert-butylamine	[47]
Rods diameter ~8 nm length ~40 nm	$0 \leq x \leq 0.2$	10 M NaOH(aq) 100 °C 20 h	$Ce(NO_3)_3 \cdot 6H_2O$ $Zr(NO_3)_4 \cdot 5H_2O$	[48]
Facetted <10 nm diameter	$0 \leq x \leq 0.2$	water 95 °C 8 h	$(NH_4)_2Ce(NO_3)_6$ $Zr(NO_3)_4 \cdot 5H_2O$ urea	[48]
Polyhedral 10–15 nm diameter	x = 0.2	water 180 °C 12 h	$Ce(NO_3)_3 \cdot 6H_2O$ $ZrO(NO_3)_2 \cdot 6H_2O$ poly(vinylpyrrolidone) hydrazine	[46]
Rods diameter ~10 nm length ~20–70 nm	x = 0.2	6 M NaOH(aq) 100 °C 24 h	$Ce(NO_3)_3 \cdot 6H_2O$ $Zr(NO_3)_4 \cdot 5H_2O$	[46]
Plates 6–12 nm diameter	x = 0.2	NH_3(aq) 100 °C 24 h	$Ce(NO_3)_3 \cdot 6H_2O$ $ZrO(NO_3)_2 \cdot 6H_2O$ CTAB [b]	[46]

[a]: A post-synthesis calcination ~600 °C was commonly applied to yield the studied product. [b]: CTAB = cetyltrimethylammonium bromide.

The high surface areas offered by small particles of ceria-zirconia prepared by solvothermal routes are suited to act as supports for precious metal nanoparticles in heterogeneous catalysis, and, indeed, some of the examples reported in Table 1 were used for this purpose, with the precious metals added in a subsequent step [46]. Taking a different approach, Das et al. used a one-step approach to prepare such catalysts, by inclusion of ruthenium chloride in the hydrothermal reaction of cerium and zirconium chlorides, with hydrazine present as a reducing agent and CTAB as a structure-influencing agent [50]. After a mild calcination, the material consisted of $Ce_{0.5}Zr_{0.5}O_2$ nanorods with a fine dispersal of Ru nanoparticles; these proved effective catalysts for the partial oxidation of methane. This illustrates how solution chemistry offers the possibility to form multicomponent systems with some control of their form.

The use of ceria as a redox catalyst in solar reactors for the upgrading of carbon dioxide and/or water to carbon monoxide and/or hydrogen in a thermochemical splitting cycle has received some attention, and the design of active materials based on ceria-zirconia has proved possible using hydrothermal synthesis. Luciani et al. showed how $Ce_{0.75}Zr_{0.25}O_2$, when prepared in 1-propanol as a solvent at 120 °C with urea as an additive, yields materials with an increase in both surface and bulk Ce^{3+}, leading to a higher oxygen mobility from and towards the catalyst surface, and, notably, even after several cycles of high-temperature treatment, these defects were maintained, leading to high activity for solar thermochemical splitting of water and carbon dioxide [44]. It should be noted that in such high-temperature applications, one possible disadvantage of materials prepared by a low-temperature solvothermal route is that any metastable composition or structure may irreversibly phase separate upon heating; this is an area in which future research is needed.

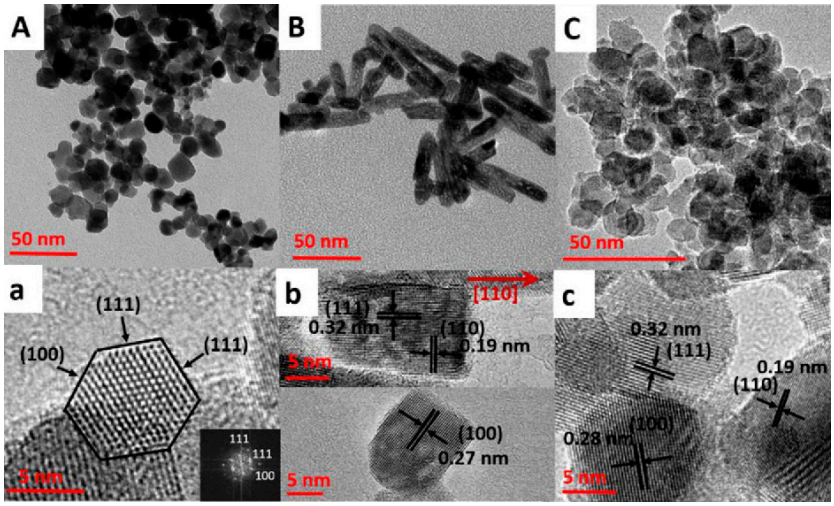

Figure 3. TEM (**top**) and HRTEM (**bottom**) images of $Ce_xZr_{1-x}O_2$ prepared using hydrothermal synthesis: (**A**,**a**) polyhedral, (**B**,**b**) rod-shaped and (**C**,**c**) plates [46]. Reprinted from Yang, Z.; Hu, W.; Zhang, N.; Li, Y.; Liao, Y. Facile synthesis of ceria–zirconia solid solutions with cubic–tetragonal interfaces and their enhanced catalytic performance in diesel soot oxidation. *J. Catal.* **2019**, *377*, 98–109, with permission from Elsevier.

Solvothermal synthesis methods lend themselves to scaling for industrial manufacture, especially when continuous flow reactors can be designed to make use of superheated solvents. Rapid-mixing devices may also be used to induce crystallisation in confined geometries, allowing control over the crystal form. Ceria-zirconia solid solutions have been prepared in this way, offering the prospect of production of catalyst materials for real application. Kim et al. used supercritical water (250 bar, 550 °C) as a reaction medium and produced fine powders of $Ce_{1-x}Zr_xO_2$ (x = 0.35, 0.5, 0.8) that were much less agglomerated than those formed by co-precipitation [51] and could be used to support Rh for catalytic reduction of NO by CO [52]. Auxéméry et al. produced nanostructured $Ce_xZr_{1-x}O_2$ ($0 \leq x \leq 0.75$) in flow reactors using an ethanol/water mixture (25 MPa, 400 °C). This yielded nanocrystallites that proved to be effective supports for Ni in dry methane reforming catalysis [53].

3.2. Transition Metal-Substituted Cerias

Through the addition of divalent (D^{2+}) and trivalent (T^{3+}) transition metal ions, compositions of the form $Ce_{1-x}D_xO_{2-x}$ or $Ce_{1-x}T_xO_{2-x/2}$, respectively, can be expected. The oxygen site vacancies that this produces can modify lattice oxide mobility, making them attractive materials for use as electrolytes in solid oxide fuel cells, and may also be of benefit in oxygen storage materials. Some transition metals are of particular interest if they can form redox pairs along with Ce^{4+}/Ce^{3+}. This is because these materials are more capable of undergoing reduction and oxidation reactions, due to the possibility of cooperative electron exchange between the two metals. This is of relevance for applications in heterogeneous catalysis. An example of this effect can be found when doping CeO_2 with CuO. The Cu^{2+}/Cu^{+} redox cycle has been shown to couple with the Ce^{4+}/Ce^{3+} pair, helping to promote the redox features [54]. These materials have also been shown to have an increased number of oxygen vacancies associated with the Cu^{2+} ions [55].

Wang et al. demonstrated that Cu-doped ceria can be synthesised hydrothermally using Ce and Cu nitrates in NaOH, heated to 180 °C for 24 h [56]. The resulting material was shown to be single phase and indexed to the $Fm\bar{3}m$ cubic space group associated with ceria. TEM showed that the synthesised particles had sizes of between 4 and 5 nm. Other groups have shown that morphology control is possible: samples with 5 and 10 mol% Cu were made using chlorides and H_2O_2 heated at 180 °C, and 5 h of heating produced

spheres with diameters of 60–80 nm, Figure 4, [57], while addition of PVP, ammonia and urea to the mixture with heating for 6 h gave spheres of ~100 nm in diameter [58].

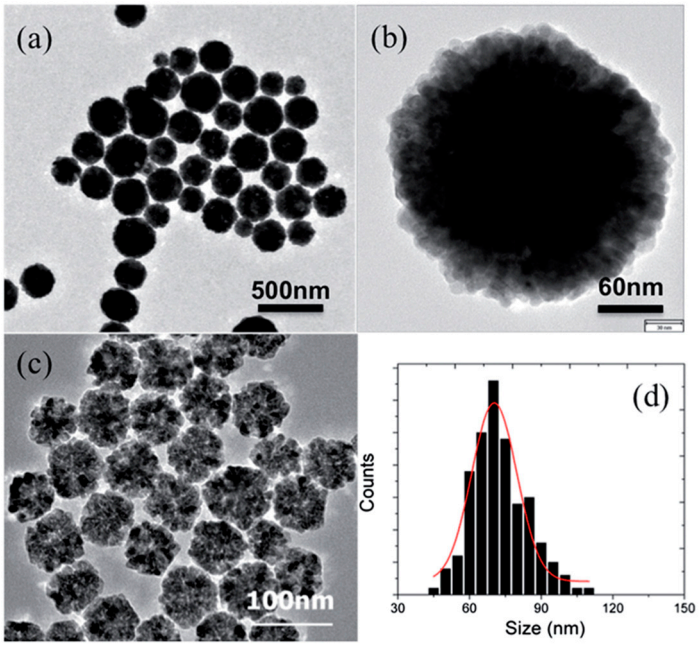

Figure 4. (**a**,**b**) TEM images of the CeO_2 nanospheres synthesised without the presence of Cu^{2+}; (**c**) TEM image of the $Cu_{0.10}Ce_{0.90}O_2$ nanospheres; (**d**) is the corresponding size distribution of the $Cu_{0.10}Ce_{0.90}O_2$ nanospheres [57]. Reproduced with permission from: Yang, F.; Wei, J.; Liu, W.; Guo, J.; Yang, Y. Copper doped ceria nanospheres: surface defects promoted catalytic activity and a versatile approach. *J. Mater. Chem. A* **2014**, *2*, 5662–5667—Published by The Royal Society of Chemistry.

Rood et al. were able to synthesise Cu-containing ceria nanotubes that were single phase up to 7 mol% Cu [59]. Their method involved using $Ce(NO_3)_3$ and $CuSO_4$ in NaOH solution heated to 100 °C for 10 h. In the same work, Cr-containing ceria nanotubes, up to a concentration of 5 mol%, were reported where a similar method was used, with $Cr(NO_3)_3$ as a precursor. These materials were tested as catalysts for both CO oxidation and NO reduction, with the Cu samples outperforming pure CeO_2 in terms of CO oxidation, but no overall improvement for NO reduction, with the Cr samples showing the opposite effect, an improvement in NO reduction, with no noticeable improvement in CO oxidation. XPS data suggested that Cu inclusion led to an increase in surface Ce^{3+}, while Cr increased the percentage of Ce^{4+} on the surface. A Cu-Cr-co-doped sample showed an improvement in conversion of CO and NO over pure ceria, and only a dopant level of 1% Cu and 1% Cr was required to reach a similar CO oxidation to a sample of 7% Cu doping, suggesting a synergistic effect in the co-doped samples. Separately, Zhang et al. showed that the catalytic performance of hydrothermally prepared Cu-CeO_2 remains constant over six cycles of CO oxidation, suggesting that the material has the potential to be a stable, recyclable oxidation catalyst [60].

Kurajica et al. produced ceria samples doped with ~10 mol% Mn, Cu or Zn from sulfate precursors and 8 M aqueous NaOH heated at 120 °C for 16 h. Elemental analysis using electron energy loss spectroscopy (EELS) and energy-dispersive X-ray spectroscopy (EDS) analysis showed that Mn substitution had occurred to the expected concentration, but the Cu and Zn concentration was lower than expected [61]. These materials appeared single phase by powder X-ray diffraction (XRD) and had average crystallite sizes between 4.2 and 6.3 nm, with Mn doped > pure ceria > Cu doped > Zn doped, as confirmed using scanning transmission electron microscopy (STEM). Prior to testing the materials' catalytic activity, the samples were fired to 500 °C to test for the presence of excess metal oxides on the surface of the materials. XRD of the materials after firing showed no extra

peaks, suggesting that the as-made samples were unlikely to have amorphous metal oxides present. A trend that was noted, with regard to crystallite size, was that the samples with larger as-made crystallites showed only minor growth relative to pure ceria, whereas the smaller as-made crystallites showed greater growth. This resulted in the Cu and Zn samples having a lower specific surface area (SSA) than pure CeO_2, while Mn had a greater SSA. To test the catalytic activity of these samples, they were used to oxidise toluene. All samples reached 50% conversion at lower temperatures than pure CeO_2.

Syed Khadar et al. demonstrated a one-step hydrothermal synthesis of 2–8 mol% Co-doped ceria [62]. Their method used $Ce(NO_3)_3$ and $CoCl_2$ in water in the presence of Na_3PO_4, heated to 180 °C for 15 h. The role of the phosphate additive was not proposed, but these nanocrystalline samples consisted of cuboid particles, which were used in their as-prepared form for their antibacterial properties. Zhang et al. hydrothermally synthesised Mn-doped CeO_2 using Ce and Mn nitrates, in a mixture of ethanol, formic acid, ammonia and peroxide heated at 150 °C for 16 h [63]. The resulting nanospheres showed single-phase XRD patterns and had an average diameter of 130 nm, as seen from electron microscopy. EDS analysis shows that there is an even distribution of all elements across the particles, Figure 5. The catalytic performance of these materials was tested to measure CO oxidation. The sample with 7 mol% Mn was cycled six times, and after an initial increase in activity at low temperatures from first to second cycle, the activity remained stable at low temperatures. The initial change in activity was associated with the removal of impurities from the surface of the nanospheres.

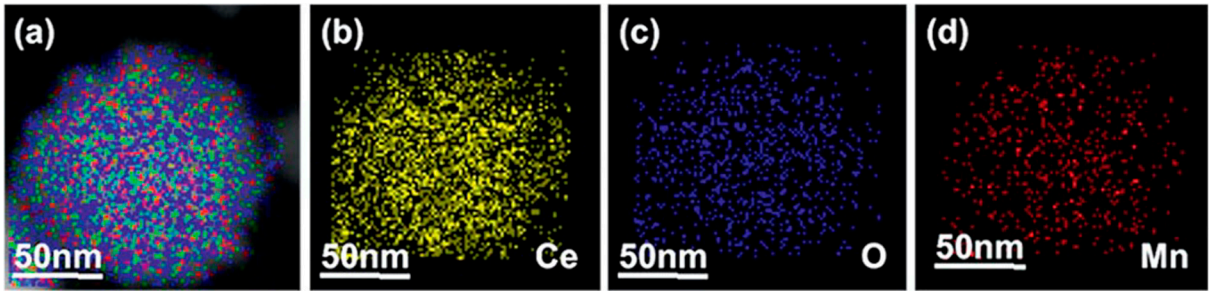

Figure 5. Energy-dispersive spectroscopy maps of a 7% Mn-substituted ceria nanosphere [63]. (**a**) shows an overlay of signals from all elements and (**b**–**d**) show the signals from individual elements. Reproduced with permission of John Wiley and Sons.

Zhang et al. produced ceria nanocubes doped with 0.5–7 mol% Mn, using nitrates and NaOH and heating to 180 °C for 24 h [64]. They observed that the size of the cubes decreased with increasing Mn concentration, but no additional peaks were observed in the XRD patterns. Temperature-programmed reduction was used to demonstrate that these materials were more reducible than pure ceria nanocubes, and the materials were used for the selective oxidation of styrene *tert*-butyl hydroperoxide.

The work of Jampaiah et al. on manganese-, cobalt- and nickel-containing ceria nanorods (10 mol% transition metal added) demonstrated that Co doping increased the concentration of surface Ce^{3+} and that these materials showed greater oxidation of CO than CeO_2 produced using the same method [65]. The reason for the formation of extremely anisotropic crystal forms, Figure 6, is not apparent, since no solution additives were employed: the synthesis method simply used nitrate salts in sodium hydroxide solution heated at 100 °C. Song et al. used a similar synthesis approach to Fe- and Co-containing ceria samples and also found rod-like crystal morphologies; in this case, beneficial activity for the catalysis for the total oxidation of propane was found [66]. Xing et al. also reported rod-shape particles upon inclusion of Mn into CeO_2 by a direct hydrothermal crystallisation [67].

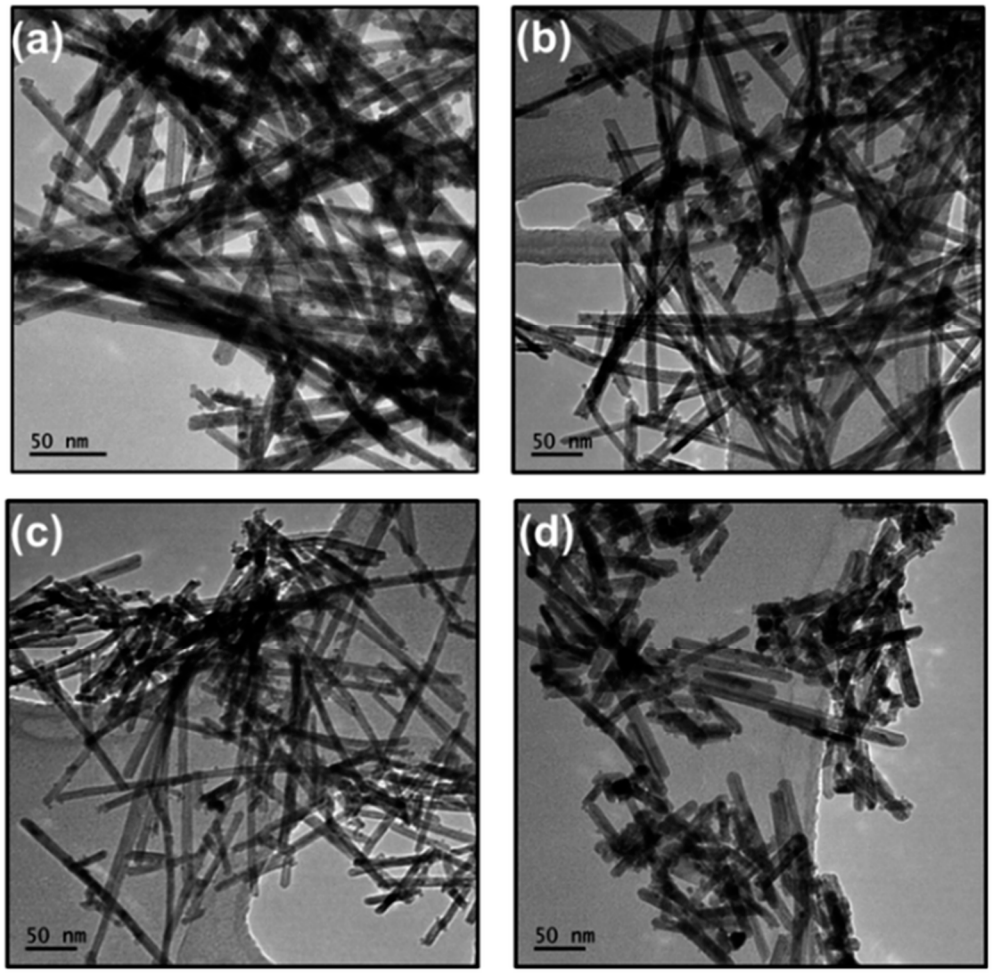

Figure 6. Nanorods of ceria materials prepared by Jampaiah: TEM images of (**a**) CeO_2, (**b**) $Ce_{0.9}Mn_{0.1}O_{2-\delta}$ (Mn–CeO_2), (**c**) $Ce_{0.9}Co_{0.1}O_{2-\delta}$ (Co–CeO_2) and (**d**) $Ce_{0.9}Ni_{0.1}O_{2-\delta}$ (Ni–CeO_2) [65]. Reproduced from Jampaiah, D.; Venkataswamy, P.; Coyle, V.E.; Reddy, B.M.; Bhargava, S.K. Low-temperature CO oxidation over manganese, cobalt, and nickel doped CeO_2 nanorods. *RSC Adv.* **2016**, *6*, 80541–80548—Published by The Royal Society of Chemistry.

Liu et al. demonstrated the synthesis of 2 mol% Co-doped nanospheres from $(NH_4)_2Ce(NO_3)_6$ and $CoCl_2$ in acetic acid and ethylene glycol heated at 180 °C for 8 h [68]. When tested as a catalyst for CO oxidation, the Co-doped sample outperformed pure CeO_2. The same method was used to prepare Ni-containing samples, and these outperformed the Co samples at CO oxidation at lower temperatures, but as the temperature increased, the Co samples reached maximum conversion faster. The work of Du et al. focussed on Ni- and Co-doped ceria nanosheets, synthesised hydrothermally using nitrates, acrylamide, glucose and ammonia, heated to 180 °C for 96 h and then fired at 400 °C for 4 h, testing the materials' ability to reduce NO [69]. It was found that the Ni-doped samples performed better, likely due to them having more oxygen vacancies than other comparable samples. Venkataswamy et al. produced CeO_2 doped at 5, 10 and 15 mol% with Cr [70]. This was achieved by mixing Ce and Cr nitrates in NaOH and heating to 100 °C for 24 h. They then fired the sample to 350 °C for 2 h. They found that the addition of Cr caused an increase in the catalytic oxidation of CO at lower temperatures up to 10 mol% The 15 mol% Cr-doped CeO_2 was shown to be less efficient than the 5 mol% sample. This is likely due to Cr being less effective as an oxidation catalyst. At lower amounts, the lattice distortion created by the dopant enhances the catalytic effect of Ce, but as the concentration increases, the loss of Ce from the sample eventually outweighs the benefit from the distortion.

Fe-substituted CeO_2 was synthesised by Phokha et al. by mixing nitrates in PVP and heating at 200 °C for 12 h [71]. They produced samples up to 7 mol% Fe that appeared single phase by XRD and Raman spectroscopy, but higher concentrations of Fe gave Fe_2O_3 as an impurity. Wang et al. were successful in producing Fe-doped ceria, up to a concentration of 20 mol% [72]. Their method involved using nitrates in ethylene glycol, heated to 180 °C for 28 h. They followed this up by heating the sample to 450 °C for 4 h. The resulting materials all matched the XRD pattern associated with CeO_2, rather than Fe_2O_3. Zheng et al. also produced Fe-doped ceria, forming the materials in a "nanoflower" morphology, Figure 7 [73]. This required mixing nitrates in urea, citric acid and ammonia, heating to 155 °C for 26 h and then firing to 500 °C for a further 3 h. The materials synthesised had an iron content of between 4 and 12 mol% and were applied for the selective oxidation of H_2S.

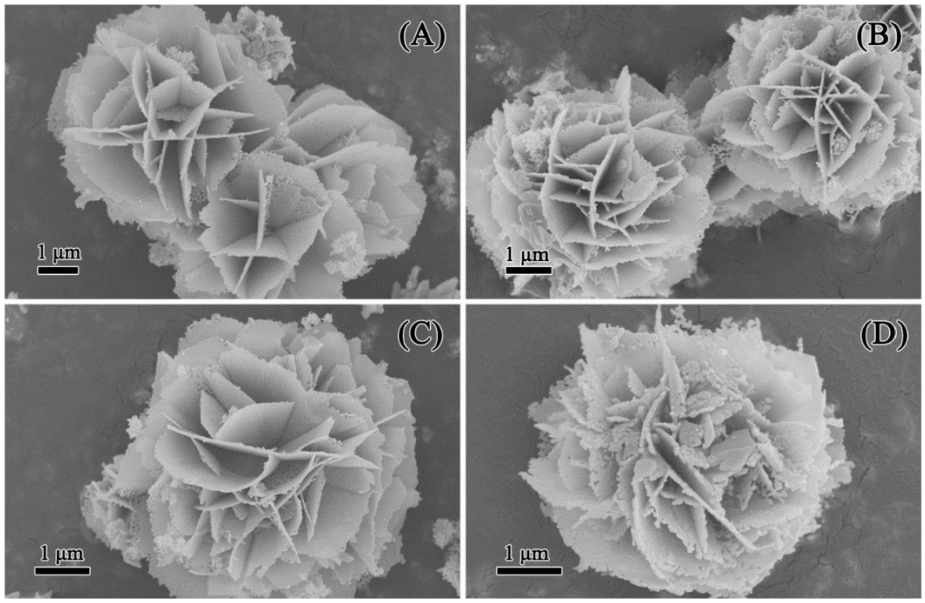

Figure 7. SEM images of Fe-containing ceria materials produced from solutions containing urea and citric acid. Fe%: (**A**) = 0, (**B**) = 4, (**C**) = 8, (**D**) = 12 [73]. Reprinted with permission from Zheng, X.; Li, Y.; Zheng, Y.; Shen, L.; Xiao, Y.; Cao, Y.; Zhang, Y.; Au, C.; Jiang, L. Highly Efficient Porous $Fe_xCe_{1-x}O_{2-\delta}$ with Three-Dimensional Hierarchical Nanoflower Morphology for H_2S-Selective Oxidation. *ACS Catal.* **2020**, *10*, 3968–3983. Copyright (2020) American Chemical Society.

The use of additives in solution has been shown to result in unusual crystal forms. In the case of Ni-containing ceria, Liu et al. used a mixed water–ethylene glycol solvent with the addition of acetic acid to form particles with spherical-like nanocluster morphology that possessed hollow centres [74]. The porosity of the particles was dependent on the volume of $Ni(NO_3)_2$ solution used in synthesis, and materials with ~6.5 mol% Ni showed high catalytic performance in carbon monoxide oxidation. Mesoporous cerium–iron binary oxides prepared by a hydrothermal technique using CTAB as a template were tested as catalysts in methanol decomposition and total oxidation of ethyl acetate: low levels of Fe were dispersed in the fluorite structure, but higher levels gave clustering of Fe and ultimately phase separation above 50% Fe [75].

As well as properties in catalysis, transition metal-substituted cerias have been prepared by hydrothermal synthesis for other applications. Barbosa et al. synthesised $Ce_{1-x}M_xO_2$ (M = Mn, Cr, Co and Fe) from aqueous sodium hydroxide solution and studied the magnetic behaviour [76]. Radović et al. synthesised ceria materials with up to 5 mol% iron by crystallisation from aqueous ammonia solution, and optical properties were studied by spectroscopic ellipsometry [77]. Fe-substituted CeO_2 prepared from nitrate salts in aqueous ammonia was found to have a high level of oxide vacancies useful for photocatalytic ozonation [78]. Recently, Fe-substituted ceria has been examined for use in rechargeable lithium batteries: $Ce_{0.9}Fe_{0.1}O_2$ was prepared by a simple hydrothermal reaction of nitrates salts in aqueous

sodium hydroxide, and its behaviour towards lithium insertion and removal was tested [79]. It was proposed that reversible reduction to metallic iron occurred on cycling, and an anode was fabricated to produce a high-powered lithium-ion battery with cycling stability and high power density; Figure 8 shows a proposal for the structural chemistry at play in this material, where the off-centring of Fe in the ideal CeO_2 structure provides space for Li insertion.

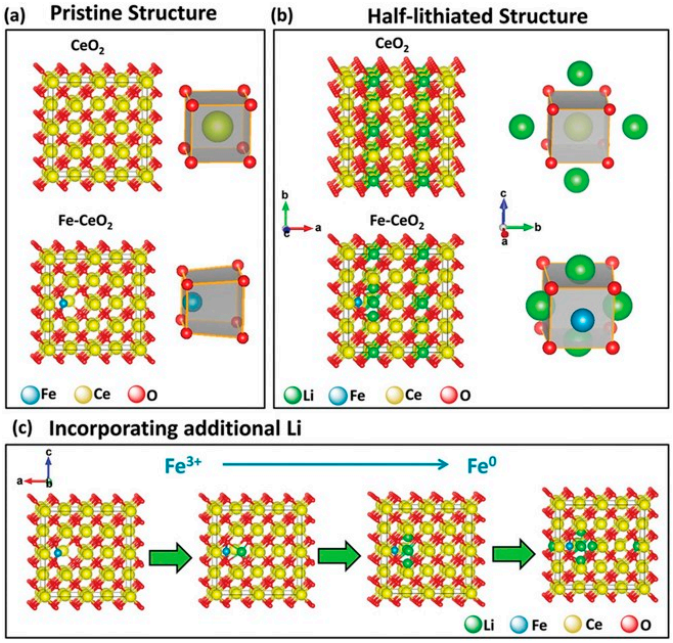

Figure 8. (**a**) Crystal structure of CeO_2 and Fe-CeO_2 and their local environments. (**b**) Prototype structure for a half-lithiated, ordered, Fe-free CeO_2, and Fe-containing structure. (**c**) Prototype structures for incorporating additional Li within the structure of Fe-containing CeO_2. Reproduced from Ma et al. [79].

Dual substitution of more than one transition metal into ceria is also of interest to tune properties. Zhang et al. prepared $Ce_{1-x}(Fe_{0.5}Zn_{0.5})_xO_{2-\delta}$ with x up to 0.018 at 200 °C and found a contraction of the lattice parameter and reduction in the crystallite size with increasing transition metal content, and XPS proved the presence of Fe^{3+} [80]. Dosa et al. prepared $Ce_{0.95}Mn_{0.025}Cu_{0.025}O_{2-\delta}$ alongside samples that contained only Cu or Mn using similar methods and found that the Mn-containing sample was more effective for soot oxidation and the Cu-containing sample showed the highest activity for CO oxidation: in this case, the co-substitution offered no benefit over CeO_2 itself [81].

A surfactant-assisted hydrothermal method was used by Zhu et al. to produce materials $Mn_xCu_yCe_{1-x-y}O_{2-\delta}$ [82]. Cetyltrimethylammonium bromide (CTAB) was added to aqueous solutions of metal salts and the pH was adjusted to 11 with NaOH before heating to 200 °C. Calcination at 550 °C yielded samples with high surface areas, >74 m^2g^1, and with evidence of mesoporosity, as seen by gas adsorption measurements. The materials showed enhanced catalytic activity for CO oxidation.

It is also worth drawing attention to the possibility of forming composite materials by hydrothermal chemistry. For example, Ji et al. produced some striking hierarchically structured particles of CuO-CeO_2 composites, Figure 9 [83]. While powder XRD showed signals from both crystalline phases, implying limited inclusion of Cu into the CeO_2 structure, electron microscopy showed an intimate association of the two phases to give composite particles of agglomerated CuO needles with surface CeO_2. Although strictly not homogeneous single phases, this work illustrates the possibilities in the preparation of novel materials with unique morphologies by choice of reagents and conditions in hydrothermal reactions.

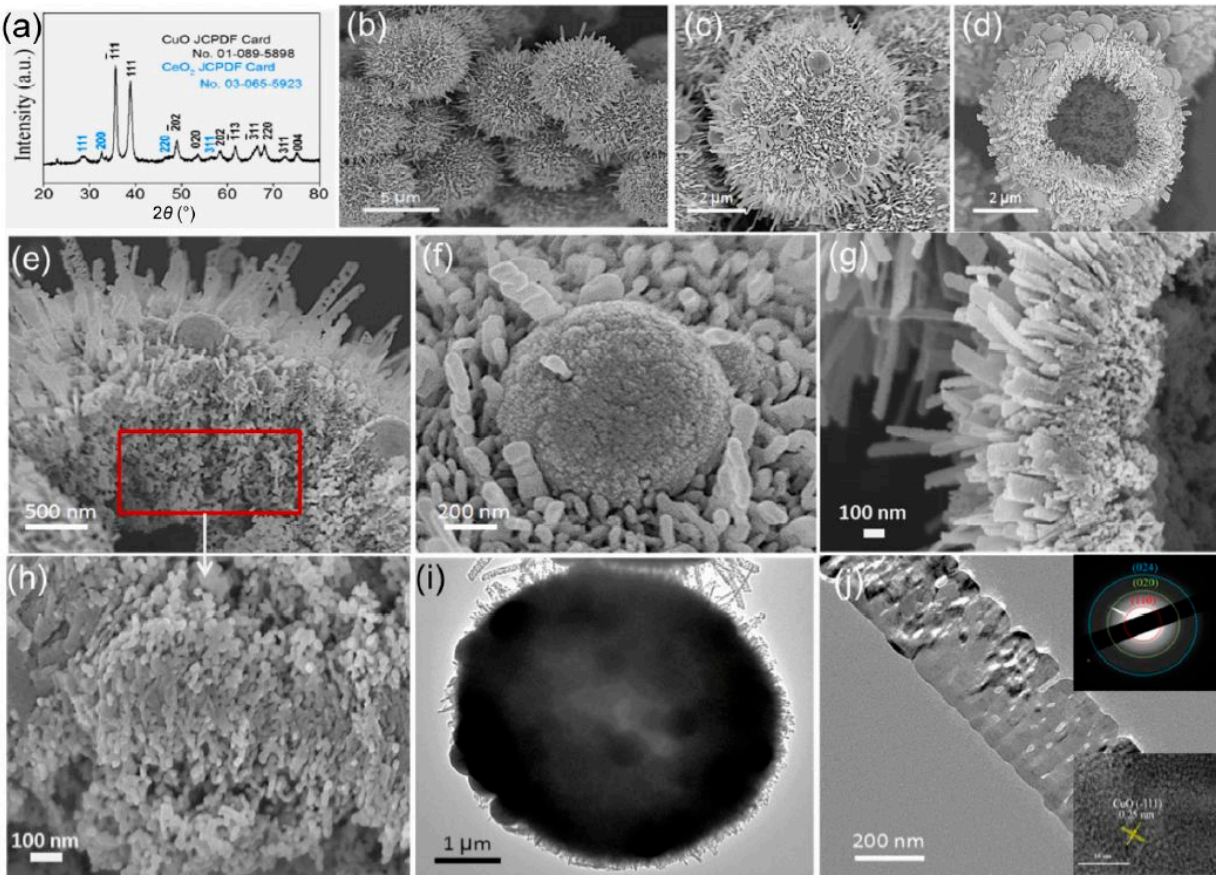

Figure 9. (**a**) Powder X-ray diffraction pattern, (**b**–**h**) FESEM images, (**i**,**j**) TEM images of CeO_2-CuO hollow microspheres. The inset of panel (**j**) (**top right**) shows the corresponding SAED pattern, with the HRTEM image of CuO nanosheets shown at the bottom right [83]. Reprinted with permission from Springer Nature Customer Service Centre GmbH: Springer. Ji, Y.; Jin, Z.; Li, J.; Zhang, Y.; Liu, H.; Shi, L.; Zhong, Z.; Su, F. Rambutan-like hierarchically heterostructured CeO_2-CuO hollow microspheres: Facile hydrothermal synthesis and applications. *Nano Res.* **2017**, *10*, 381–396.

As described thus far, much of the work on transition metal substitution has focussed on the first-row series, and few examples of inclusion of the second-row and third-row elements in ceria by solvothermal routes have also been proven. The case of precious metals is important to consider since ceria is often used as a support for precious metal particles. Hiley et al. showed the inclusion of Pd^{2+} into the cubic fluorite structure of CeO_2 was possible for up to 20 mol% substitution from $CeCl_3{\cdot}7H_2O$ and $PdCl_2$ in aqueous $NaOH/H_2O_2$ [84]. As well as inducing charge-balancing oxide vacancies, the square planar preference of Pd^{2+} induces a structural distortion, as evidenced from EXAFS spectroscopy, Figure 10a. This material is unstable on heating in air above 700 °C, and the Pd is extruded to give metallic particles on CeO_2, which is, in itself, of interest for heterogeneous catalysis. The case of niobium substitution is an interesting situation as its preferred oxidation of +5 requires a different charge-balancing mechanism than substituents with lower charge. Hydrothermal synthesis from $NbCl_5$ and $CeCl_3{\cdot}7H_2O$ in aqueous NaOH solutions produced substituted ceria materials in which charge compensation was achieved by co-inclusion of Na^+ to give materials of composition $(Ce_{1-x}Nb_x)_{1-y}Na_yO_{2-\delta}$ (where $x \leq 0.30$ and $y \geq \sim x/3$) [85]. Here, neutron pair distribution function analysis showed how the lower coordination number preference of Nb^{5+} leads to a local distortion of the structure, Figure 10b, which can be used to explain the enhanced oxygen storage properties of the material.

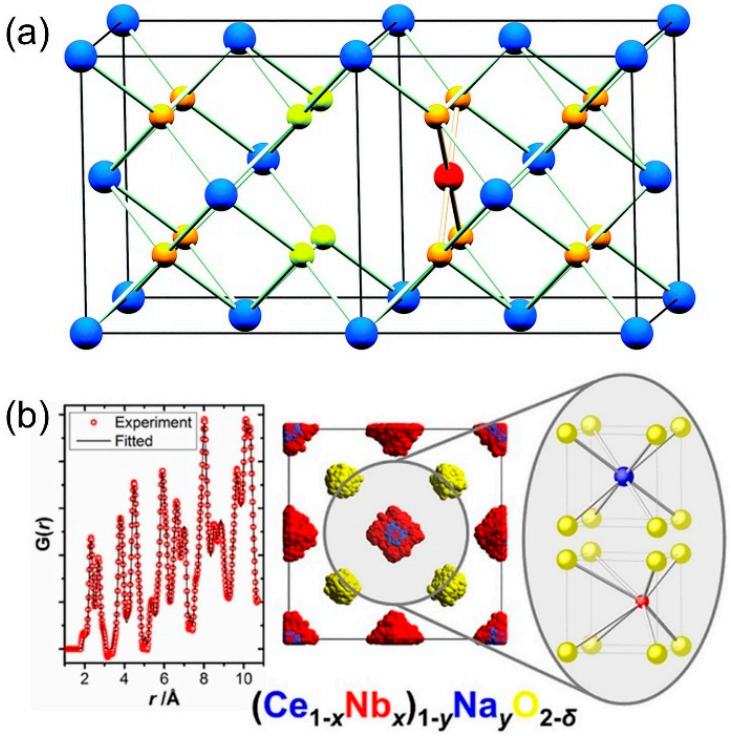

Figure 10. Local environment of (**a**) Pd^{2+} and (**b**) Nb^{5+} in substituted ceria materials prepared by hydrothermal synthesis. In (**a**), cerium is represented by the blue spheres, Pd by the red and the oxide anions by orange or yellow, with the oxide anions being adjacent to a vacant Ce site caused by the square planar preference of Pd^{2+} [84]. In (**b**), the left panel shows the fitted pair distribution function used to derive the structural model shown on the right, where the colour scheme is indicated by the chemical formula [85]. (**a**) Reproduced from Hiley, C.I.; Fisher, J.M.; Thompsett, D.; Kashtiban, R.J.; Sloan, J.; Walton, R.I. Incorporation of square-planar Pd^{2+} in fluorite CeO_2: hydrothermal preparation, local structure, redox properties and stability. *J. Mater. Chem. A* **2015**, *3*, 13072–13079—Published by The Royal Society of Chemistry. (**b**) Reprinted with permission from Hiley, C.I.; Playford, H.Y.; Fisher, J.M.; Felix, N.C.; Thompsett, D.; Kashtiban, R.J.; Walton, R.I. Pair Distribution Function Analysis of Structural Disorder by Nb^{5+} Inclusion in Ceria: Evidence for Enhanced Oxygen Storage Capacity from Under-Coordinated Oxide. *J. Am. Chem. Soc.* **2018**, *140*, 1588–1591. Copyright (2018) American Chemical Society.

3.3. Main Group Substituents

The main group elements include those from the s and p blocks of the periodic table and cover a wide range of possible substituents for cerium dioxide, ranging from the hard cations of Groups 1 and 2 to the more covalently bound atoms from the p block. Hydrothermal synthesis provides a convenient way to explore this substitutional chemistry since phases that might otherwise phase separate during high-temperature synthesis may crystallise to yield unique compositions with unusual structural features and, potentially, properties.

From the alkali earths in Group 2, Ma et al. reported magnesium-containing materials $Ce_{1-x}Mg_xO_2$ (x = 0.00, 0.02, 0.04, 0.06, 0.08) in the form of nanowires, prepared in a water–ethylenediamine mixture with NaOH as a mineraliser and $CeCl_3{\cdot}7H_2O$ and $MgCl_2{\cdot}2H_2O$ heated at 180 °C for 14 h [86]. Calcium- and strontium-containing CeO_2 with nominal compositions $Ce_{0.90}Ca_{0.10}O_{1.90}$, $Ce_{0.90}Ca_{0.05}Sr_{0.05}O_{1.90}$ and $Ce_{0.90}Sr_{0.10}O_{1.90}$ was prepared from Ce(III) nitrate and salts of Ca^{2+} and Sr^{2+} in aqueous NaOH at pH = 14, heated at 220 °C for up to 8 h [87]. Only a low level of incorporation of Sr into the ceria structure was found, explained by the larger size of Sr^{2+} compared to Ce^{4+}. The small crystal size (12–16 nm) of the powders allowed effective sintering into dense ceramic pellets at 1350 °C for 5 h, and for the Sr-containing material, a secondary phase of $SrCeO_3$ was then seen,

consistent with the fact that Sr is not effectively incorporated into ceria. The Ca-containing sample showed favourable ionic conductivity after sintering.

From Group 12, zinc-containing ceria with up to 20% of the cerium replaced by the substituent was prepared by a continuous hydrothermal synthesis approach using supercritical water as a reaction medium (450 °C and 24.1 MPa) and KOH as a mineraliser. The samples were formed as nanocrystalline powders with crystallite sizes less than 5 nm [88]. A 10% Zn-containing CeO_2 was found to be an effective catalyst for the CO_2 hydrogenation reaction, ascribed to the highest level of Ce^{3+} defects [89]. Although not an elemental substitution, the formation of ZnO-CeO_2 heterojunctions by hydrothermal synthesis has also been studied, where the purposeful growth of the two phases in intimate contact leads to superior visible-light photocatalytic performance [90].

Of the Group 13 elements, only indium has been introduced in ceria via hydrothermal conditions. Younis et al. published a synthesis of indium-containing CeO_2 that appears single phase up to 15 mol% In [91]. This involved mixing aqueous solutions of Ce and In nitrates and adding toluene, oleic acid and *tert*-butylamine. The reaction mixture was heated to 200 °C for 36 h and the solid product calcined at 180 °C for 1 h. The lattice parameters of the synthesised samples decreased with increasing In^{3+} concentration, attributed to the smaller ionic radius of In. The 5 and 10 mol% In samples outperformed pure CeO_2 in the photocatalytic degradation of organic dyes.

From Group 14, the inclusion of Sn and Pb into CeO_2 has been examined by solvothermal routes. Abbas et al. produced phase-pure samples on Sn-containing ceria up to 7% Sn, designed for use as a cytotoxic nanomedicine using $Ce(NO_3)_3$ and $SnCl_2$ in polyethylene glycol and NaOH heated to 95 °C for 12 h and then fired to 300 °C for 2 h [92]. The addition of Sn changed the morphology of the material from spherical nanoparticles to a heterogeneous nanowires–nanosheets structure. A contraction of the unit cell was reported, although the oxidation state of Sn was not measured. Shajahan et al. successfully synthesised single-phase Pb-containing CeO_2 using nitrates in NaOH, heated to 140 °C for 14 h followed by heat treatment at 350 °C for 3 h [93]. The samples appeared single phase under XRD in samples up to 12% Pb, and it was found that up to 6% Pb, the band gap of the material was lower, making it a better photocatalyst than pure ceria, while higher Pb content increased the materials' bandgaps. The oxidation state of Pb was proved to be +2 using X-ray photoelectron spectroscopy.

From the elements in Group 15, there are several examples of how Bi^{3+} has been studied as a way of modifying CeO_2, and hydrothermal synthesis allows a convenient route to the introduction of high levels of substitution with up to 60% of the cerium replaced. The hydrothermal oxidation of Ce^{3+} in basic aqueous solution by $NaBiO_3$ at 240 °C provides a redox synthetic method, where the product phase contains Ce^{4+} and Bi^{3+}, to form nanocrystalline powders (Figure 11) that show high reducibility, although the extrusion of the Bi metal will limit the practical application of the materials [94]. Bi-substituted CeO_2 has frequently been investigated for use in photocatalysis, although it has also been looked at for uses such as antibacterial activity: Frerichs et al. produced single, cubic-phase samples up to 20 mol% Bi by reacting Bi and Ce nitrates in NaOH and heating to 80 °C for 25 h [95]. Samples made using a higher level of Bi were a two-phase mix of the cubic CeO_2 structure and the monoclinic Bi_2O_3 material. Houlberg et al. synthesised materials using $Bi(NO_3)_3$ and $(NH_4)_2Ce(NO_3)_6$ in NaOH, heated to 200 °C for 20 h, and produced samples that were single cubic phase up to 60% Bi [96]. This study employed in situ X-ray diffraction to track the formation of the product and proved that mixed metal oxide phases were formed at the earliest stages of reaction even before heating under hydrothermal conditions. Other methods that have been used to create phase-pure samples up to ~10% Bi have been reported. Shanavas et al. used nitrates in NaOH, heated to 140 °C for 14 h and then firing at 350 °C for 3 h to remove surface impurities [97]. Veedu et al. used nitrates in ammonia and HCl, heated to 100 °C and then firing to 500 °C [98].

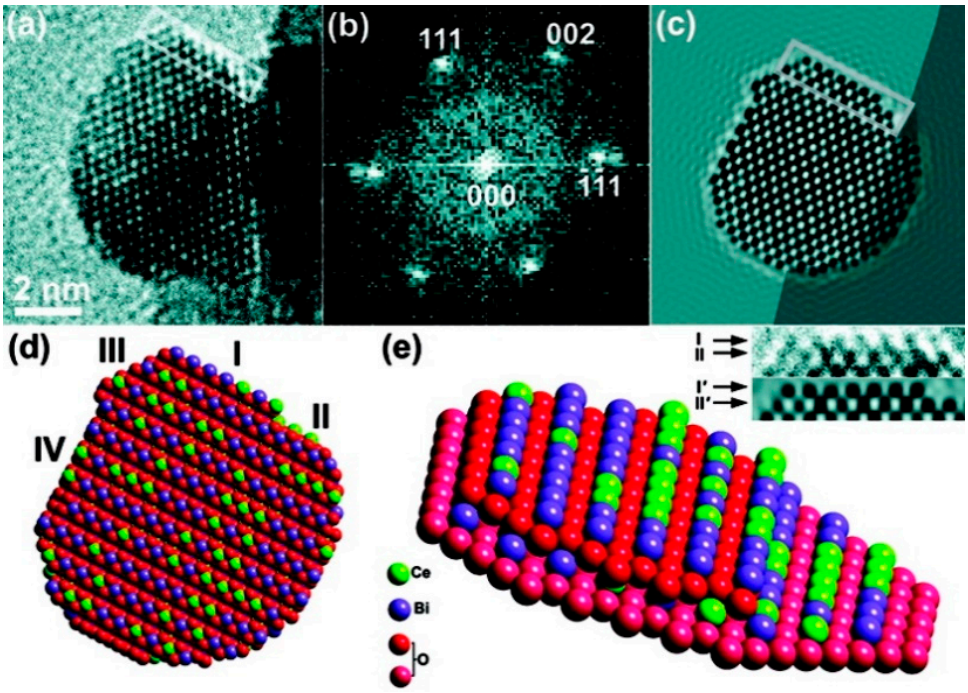

Figure 11. (**a**) High-resolution TEM image of a faceted crystallite of $Ce_{0.5}Bi_{0.5}O_{1.75}$ with one facet highlighted. (**b**) Indexed FFT obtained from the lattice image in Part (**a**). (**c**) A multislice image simulation produced for a similar fragment as in (**a**) with the same facet highlighted. (**d**) Faceted structure model used to produce the simulation in (**c**). I, II, III and IV indicate (002), (002)′, (111) and (220) facets, respectively, assigned relative to (**b**). (**e**) Schematic surface structure model showing the (002) step and (002) terrace. Insets are details from the corresponding lattice image (i.e., I and II) and simulation (i.e., I′ and II′). Surface oxygens are omitted for clarity [94]. Reprinted with permission from Sardar, K.; Playford, H.Y.; Darton, R.J.; Barney, E.R.; Hannon, A.C.; Tompsett, D.; Fisher, J.; Kashtiban, R.J.; Sloan, J.; Ramos, S.; Cibin, G.; Walton, R.I. Nanocrystalline Cerium−Bismuth Oxides: Synthesis, Structural Characterization, and Redox Properties. *Chem. Mater.* **2010**, *22*, 6191–6201. Copyright (2010) American Chemical Society.

Unlike bismuth, which is found in the +3 oxidation state when included in ceria, the earlier member of Group 15, antimony, has been shown to be present in the +5 oxidation state: this is the case whether $SbCl_3$ or $SbCl_5$ is used under hydrothermal conditions in the presence of NaOH and H_2O_2 [99]. Here, like the case of niobium mentioned above, the co-substitution of sodium is found to balance the charge of the pentavalent substituent, resulting in chemical formulae $(Ce_{1-x}Sb_x)_{1-y}Na_yO_{2-\delta}$ (where $x < 0.4$ and $y \geq x/3$). As with bismuth, the antimony-containing samples are unstable in highly reducing conditions and phase separate to yield elemental antimony.

Finally, we consider a more unusual case, where nitrogen can partially replace oxygen in CeO_2 to give an oxynitride analogue of ceria. Xu and Li produced samples from $Ce(NO_3)_3$ and $(NH_4)_2S_2O_8$ in water heated to 200 °C for 24 h [100]. XRD recorded before and after a calcination at 500 °C for 2 h shows that the sample adopts the cubic ceria structure, with no additional peaks visible. Large excesses of nitrogen, from the ammonium persulfate reagent, were needed to achieve substitution, but the highest Ce/N ratio achieved in the product was 1:0.052, which is close to the solid solubility limit. The lattice parameters of all doped samples were larger than the expected value for pure Ce, due to the lattice distortion caused by the N^{3-} being larger than O^{2-}. This was found to enhance the oxygen storage capacity of these materials.

3.4. Rare Earth-Substituted Ceria

The inclusion of rare earths (the other lanthanides and yttrium) into ceria has attracted much attention by various synthetic approaches, and these include numerous solvothermal

routes. All of the available rare earths have been studied in this respect and a complete survey of materials prepared solvothermally in the past decade are included as Supporting Information (Table S1). Typically, up to 50% of the Ce can be replaced by a trivalent substituent, before impurity phases, such as $Ln(OH)_3$ or LnO(OH), are seen, particularly for the rare earths with smaller ionic radii [101–103]. Most synthesis is performed under hydrothermal conditions from aqueous solutions of metal salts: typically nitrates of the trivalent cations, but occasionally chlorides or acetates, and in the case of cerium, Ce(IV) salt $(NH_4)_2Ce(NO_3)_6$ has also been used. In the simplest cases, the pH is increased by addition of NaOH, KOH or ammonia, and temperatures spanning 80–250 °C have been reported to produce a solid product. In many cases, the solid formed is crystalline, but often a subsequent heat treatment up to 500 °C is applied, simply to remove any surface-bound species. Under these conditions, the typical morphology of CeO_2 itself is of cube-shaped crystallites, Figure 12 [104], which may appear spherical when the size is 10 nm or less. The size of the crystals may depend on pH, temperature and time of reaction.

Upon introduction of small amounts of a second lanthanide, the cube-shaped crystal is usually maintained, but it has been reported that at higher substituent levels, and under otherwise identical reaction conditions, the crystal morphology becomes increasingly rod-shaped, with a distribution of both crystal forms at intermediate compositions. This is exemplified by the case of praseodymium, where the same phenomenon has been reported independently by several different research groups: [105–108] at 25% Pr substitution and above, the rod-like crystal morphology is detected, and an example is shown in Figure 13. Praseodymium may also be found in the +4 oxidation state, and this has been inferred from the redox properties of some of these samples [106,108] and detected by X-ray spectroscopy in others [105,107]. This, however, does not explain the formation of the rod-like crystallites. Interestingly, Mendiuk et al. found for Ln = Pr, Sm, Gd, Tb, at higher Ln substitutions, the formation of $Ln(OH)_3$ rod-like crystals [109]. It may well be possible that the formation of these anisotropic crystallites has a seeding effect in the subsequent growth of the oxide, or that when a second step of firing is applied, even at moderate temperature, the dehydration of the hydroxide occurs with retention of crystal morphology. Consistent with this idea, Hong et al. separately showed the anisotropic crystallites of phase-pure $(Ce,Gd)(OH)_3$ could be dehydrated to the mixed oxide on heating at just 400 °C with crystal morphology maintained [110]. Yoshida and Fujihara found that for Sm substitution, hydrothermal treatment at 100 °C prior to heat treatment gave rod-shaped crystals, even for very low Sm content, which may imply the initial formation of a hydroxide phase at mild conditions [111].

Regarding crystallisation mechanisms, Mendiuk et al. proposed that for the cube-shaped crystallites, their assembly occurred by an oriented attachment mechanism, owing to the observation of a bimodal crystallite size distribution [102,109]. A careful study of Sm-CeO_2 nanocubes using spatially resolved electron energy loss spectroscopy on the TEM showed the that presence of the Ln^{3+} substituent did not affect the Ce^{3+} concentration at the surface of the crystallites [112].

The addition of solution additives has been explored as a way to modify the crystal morphology of lanthanide-substituted materials. In one of the simplest cases, Ke et al. added NaCl to the crystallisation of a set of lanthanide-substituted cerias (Ln = La-Lu with 10 mol% substituent) from chloride precursors in 12 M NaOH and found nanowires ~5 nm in diameter with an aspect ratio of ~500, Figure 14 [113]. In the processing of these samples, heating to only 300 °C was performed, which does imply that the ionic strength of the solution may play a role in the crystallisation process.

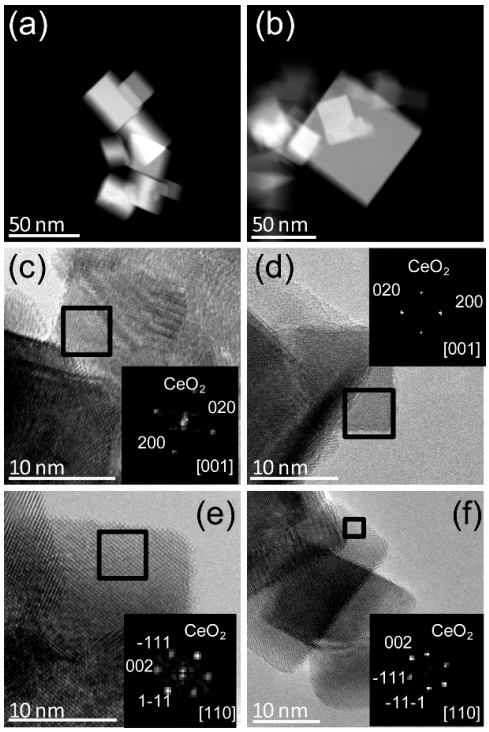

Figure 12. HAADF-STEM images of (**a**) CeO_2 nanocrystals and (**b**) 10% La-CeO_2 nanocrystals; HREM images of (**c**,**e**) CeO_2 nanocrystals and (**d**), (**f**) 10%La-CeO_2 nanocrystal samples in the [001] and [110] zone axis [104]. Reprinted with permission from Fernandez-Garcia, S.; Jiang, L.; Tinoco, M.; Hungria, A.B.; Han, J.; Blanco, G.; Calvino, J.J.; Chen, X. Enhanced Hydroxyl Radical Scavenging Activity by Doping Lanthanum in Ceria Nanocubes. *J. Phys. Chem. C* **2016**, *120*, 1891–1901. Copyright (2016) American Chemical Society.

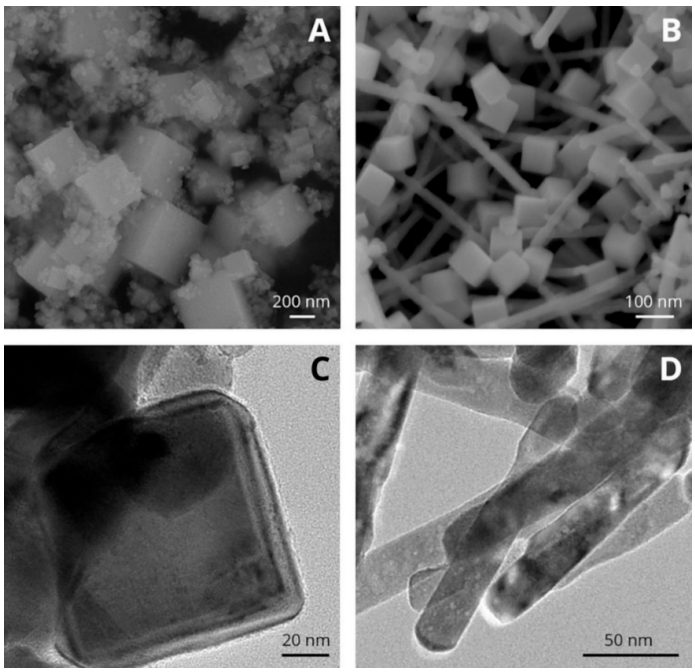

Figure 13. FE-SEM and TEM images of CeO_2 (**A**,**C**) and 50% Pr-CeO_2 (**B**,**D**) [107]. Reprinted from Andana, T.; Piumetti, M.; Bensaid, S.; Veyre, L.; Thieuleux, C.; Russo, N.; Fino, D.; Quadrelli, E.A.; Pirone, R. Nanostructured equimolar ceria-praseodymia for NO*x*-assisted soot oxidation: Insight into Pr dominance over Pt nanoparticles and metal–support interaction. *Appl. Catal. B Environ.* **2018**, *226*, 147–161, with permission from Elsevier.

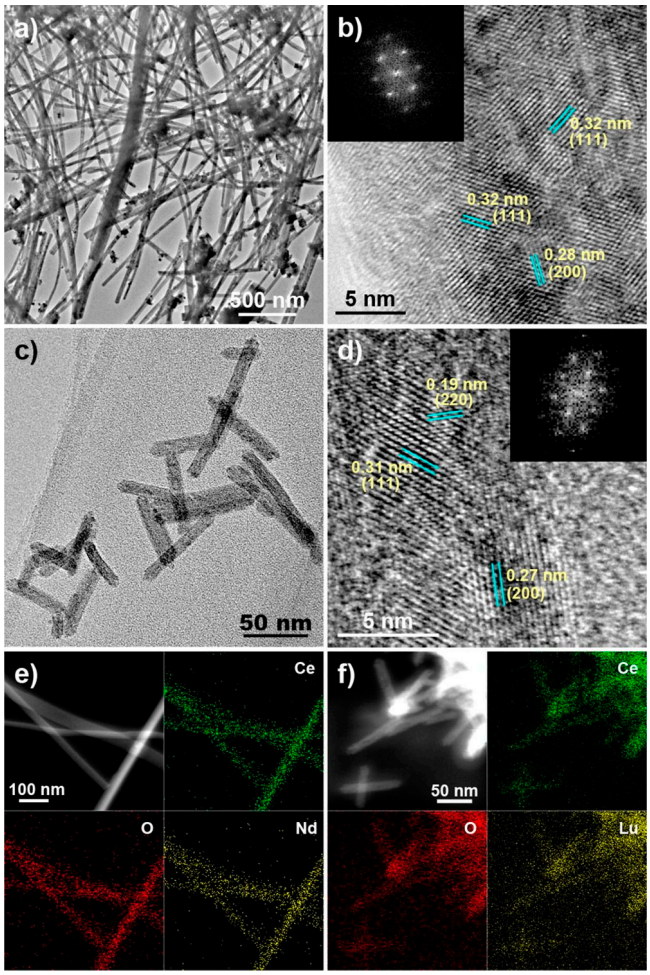

Figure 14. TEM (**a**,**c**), HRTEM (**b**,**d**) and HAADF-STEM EDS elemental mapping (**e**,**f**) images of CeO_2:Nd (**a**,**b**,**e**) and CeO_2:Lu nanocrystals (**c**,**d**,**f**). Insets in Panels (**b**) and (**d**) are the fast Fourier transition analyses, indicating that (110) surfaces are exposed for both samples. In Panels **e** and **f**, the up-left images are the HAADF-STEM images. The upper right and bottom left and right ones in Panels (**e**,**f**) are the EDS elemental mapping images representing Ce, O and the dopant (Nd for panel (**e**) and Lu for panel (**f**)) [113]. Reprinted with permission from Ke, J.; Xiao, J.-W.; Zhu, W.; Liu, H.; Si, R.; Zhang, Y.-W.; Yan, C.-H. Dopant-Induced Modification of Active Site Structure and Surface Bonding Mode for High-Performance Nanocatalysts: CO Oxidation on Capping-free (110)-oriented CeO_2:Ln (Ln = La–Lu) Nanowires. *J. Am. Chem. Soc.* **2013**, *135*, 15191–15200. Copyright (2013) American Chemical Society.

An additive that has been well established to affect crystal morphology in hydrothermal formation of cerium oxides is $Na_3PO_4{\cdot}12H_2O$. Xu et al. found for yttrium substitution that octahedral crystals were produced but with surface nanorods with increasing addition of sodium phosphate [114]. The same octahedral crystal morphology was found by Małecka et al., who studied the formation of ytterbium-substituted CeO_2 [103,115], Roh et al., who examined europium substitution [116], Bo et al. for Er-CeO_2 [117] and Yang et al., who prepared erbium-substituted materials, some of which were co-substituted with lithium, Figure 15, where morphology is maintained even after a high-temperature annealing of 800 °C [118]. Małecka also observed that rod-shaped crystals were found at high concentrations of $Na_3PO_4{\cdot}12H_2O$ [115]. The octahedral morphology, bounded by {111} faces, is known to be a stable form for large crystals of CeO_2 itself [119], and while earlier work showed the effectiveness of Na_3PO_4 as a mineraliser for growth of octahedral nanocrystals of CeO_2, the mechanism of this precise morphological control

has not been established, beyond discussion of how it might control pH and affect the dissolution–recrystallisation processes leading to crystallisation [120].

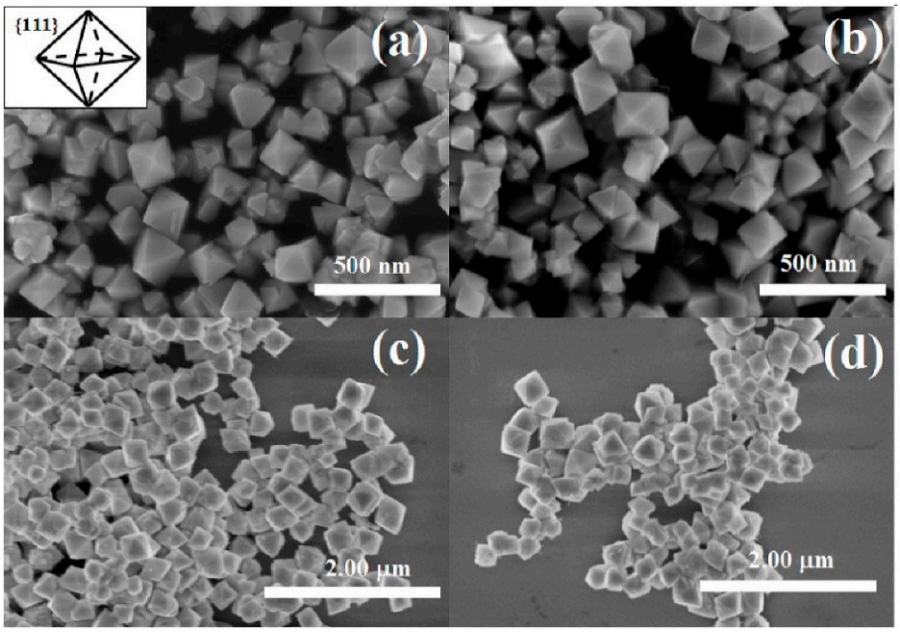

Figure 15. Octahedra of Er-CeO_2 prepared using $Na_3PO_4{\cdot}12H_2O$ as an additive in hydrothermal crystallisation (**a**), CeO_2: 3 mol% Er^{3+}, 10 mol% Li^+ (**b**) and the SEM images of the above nanocrystals with post-calcination temperatures of 800 °C (**c**,**d**) [118]. Reprinted from Yang, Y.; Cong, Y.; Dong, D.P.; Xiao, Y.; Shang, J.Y.; Tong, Y.; Zhang, H.M.; He, M.; Zhang, J.H. Structural and excitation dependent emission properties of octahedral CeO_2:Er^{3+} nanocrystal. *J. Lumin.* **2019**, *213*, 427–432, with permission from Elsevier.

Urea has been investigated as an additive for when crystallising ceria with substituents Pr, Gd [121] and Tb [122,123], and this may be observed to have the general effect of forming small, ~10 nm, crystallites that are often agglomerated. Muñoz et al. used microwave heating (see below) and produced Gd-CeO_2 materials that consisted of spherical assemblies of the primary particles, Figure 16. The combination of urea and sodium citrate was studied by Xu et al. for La, Nd, Sm and Eu substitution, who found "broom-like" agglomerates of needle-like crystals [124]. Urea is known to decompose under hydrothermal conditions into ammonium and cyanate, and this has been speculated to control the nucleation by pH control, in the case of ceria itself leading to smaller crystallites at higher urea concentrations [125].

Other additives that have been investigated for control of crystal morphology of substituted cerias include hexamethylenetetramine [126–128] and tetramethyl ammonium hydroxide [129–131]. The role of these additives has not been determined, and often simply the outcome of their influence on crystal morphology is described. Sato et al. speculated that tetramethylammonium ions cap the growing crystal faces of Gd-CeO_2 to avoid agglomeration and ripening, thus forming cuboidal crystals of only 4 nm in dimension [131].

Mixtures of additives have also been investigated, such as polyvinylpyrrolidone, HCl, $KClO_3$ and *N*,*N*-dimethylformamide [132], octadecylamine, ethanol and ethylenediamine [133] or 6-amino hexanoic acid and *tert*-butylamine [134], and non-aqueous solvents have been studied, such as ethylene glycol [135–138], ethanol [139] and triethylene glycol [140]. In some cases, the choice of combination of additive and solvent has led to some striking crystal morphologies; for example, the combination of epigallocatechin-3-gallate in ethanol as a solvent allowed the formation of hierarchical nanostructures of Eu-containing CeO_2 with flower-like shapes of intergrown plates, microns in thickness, Figure 17 [141].

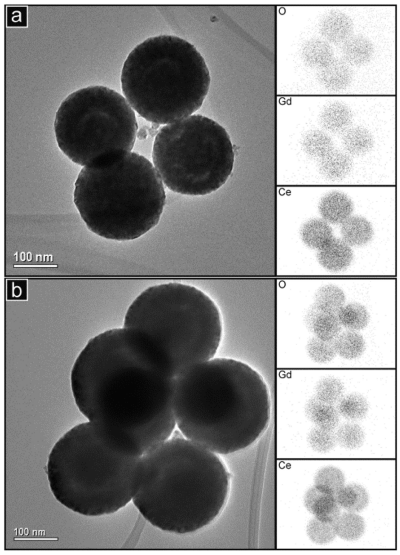

Figure 16. TEM images of groups of spherical particles of gadolinium-substituted CeO_2 prepared in the presence of urea with (**a**) 10% Gd and (**b**) 20% Gd, with corresponding energy-dispersive spectroscopy maps of the elements shown on the right [121]. Reproduced from Muñoz, F.F.; Acuña, L.M.; Albornoz, C.A.; Leyva, A.G.; Baker, R.T.; Fuentes, R.O. Redox properties of nanostructured lanthanide-doped ceria spheres prepared by microwave assisted hydrothermal homogeneous co-precipitation. *Nanoscale* **2015**, *7*, 271–281—Published by The Royal Society of Chemistry.

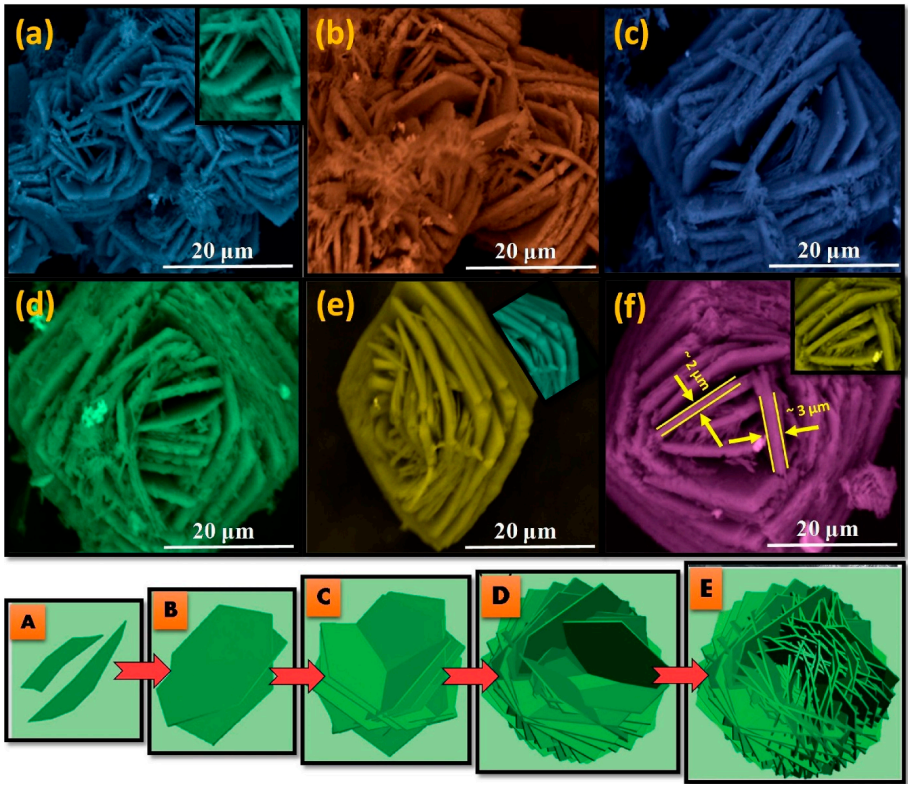

Figure 17. EM images of CeO_2:Eu^{3+} (3 mol%) NPs prepared with different reaction times in ethanol (**a**) 2 h, (**b**) 4 h, (**c**) 6 h, (**d**) 8 h, (**e**) 10 h and (**f**) 12 h with 30% *w*/*v* of EGCG at 180 °C, and (**A**–**E**) depict the proposed growth mechanism of the hierarchical morphology. EGCG is epigallocatechin-3-gallate [141]. Reprinted from Deepthi, N.H.; Darshan, G.P.; Basavaraj, R.B.; Prasad, B.D.; Nagabhushana, H. Large-scale controlled bio-inspired fabrication of 3D CeO_2:Eu^{3+} hierarchical structures for evaluation of highly sensitive visualization of latent fingerprints. *Sens. Actuators B Chem.* **2018**, *255*, 3127–3147, with permission from Elsevier.

As well as conventional heating, microwaves have been used to facilitate solvothermal crystallisations of rare earth-substituted cerias. The advantage here lies in the short reaction times, from a few hours down to just a few minutes [102,103,115,121–123,128,142–146].

Continuous flow synthesis has also been used for some rare earth-substituted ceria materials. Slostowski et al. produced La- and Pr-substituted ceria in a custom-built, continuous flow reactor in supercritical water, up to 400 °C, and formed crystallites less than 10 nm in size, observing that higher temperature allowed a higher level of element substitution [147]. Xu et al. used supercritical water at 396 °C and rapid mixing, ~29 s, with solutions of metal salts and KOH to yield Gd-CeO_2 [148]. Their apparatus, Figure 18, had a further two stages of heating points before allowing the product to be tapped as a slurry. Depending on pH, the crystallites produced were between 6 and 40 nm in size with a polyhedral or octahedral shape.

Applications of rare earth-substituted ceria materials span the types of fields expected for these materials, from oxide ion conductors in solid oxide fuel cells, where the enhanced sinterability of fine powders into ceramics is beneficial [136,137,143,149,150], to catalysts for CO and soot oxidation, where the high surface and exposure of specific crystal faces may offer some benefits [103,105,107,108,113,115,132,133,135,150–153]. Photocatalytic properties are of increasing focus for degradation of pollutants or organic transformations, and some of the rare earth-substituted materials have been screened for these applications [101,124,141,154].

Photoluminescence is a property that has commonly been used to characterise rare earth-substituted ceria materials [111,114,117,144,155–160], while Eu-substituted materials are of particular interest for their luminescent properties. Eu-CeO_2 materials prepared by solvothermal routes have provided some useful materials: this includes in applications such as solar cells, Figure 19 [116], and detection of fingerprints [141]. The use of solvothermal conditions to prepare nanocrystals of ceria materials has allowed specimens to be prepared for study of their toxicity: Dunnick et al. used gadolinium-substituted samples and examined their properties in vivo in rats [129,130].

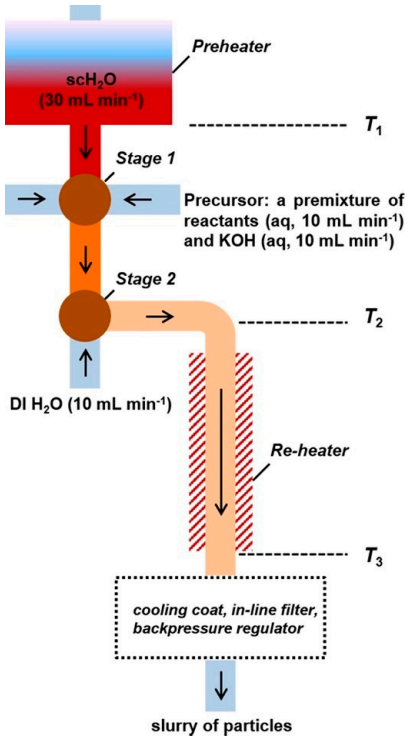

Figure 18. A schematic representation of the two-stage continuous hydrothermal flow synthesis reactor used by Xu et al. for the preparation of Gd-CeO_2 using pressure controlled at 26 MPa. The flow rate of each H_2O/solution stream is given in parentheses; arrows indicate the flow direction [148]. Reproduced with permission from John Wiley and sons.

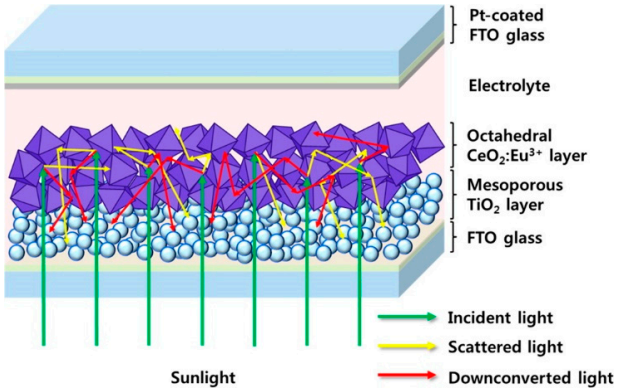

Figure 19. Schematic of a bilayer dye-sensitised solar cell device fabricated from hydrothermally synthesised octahedral CeO_2:Eu^{3+} nanocrystals for light scattering and down conversion [116]. Reprinted with permission from Roh, J.; Hwang, S.H.; Jang, J. Dual-Functional CeO_2:Eu^{3+} Nanocrystals for Performance-Enhanced Dye-Sensitized Solar Cells. *ACS Appl. Mater. Interfaces* **2014**, *6*, 19825–19832. Copyright (2014) American Chemical Society.

In terms of practical applications, the formation of composites is of relevance, and the solvothermal routes have allowed some useful possibility of accessing novel materials with practical applications. Pr-doped CeO_2 nanorods were introduced into a Sr-doped $LaMnO_3$–Y_2O_3-stabilized ZrO_2 composite by an in situ hydrothermal growth process: this gave an enhanced performance of the material for use as an electrode in solid oxide fuel cell applications [161]. Jiang et al. produced gadolinium-substituted ceria crystallites on a graphene support, by including the support material in the hydrothermal reaction [162]. This was tested for application in non-aqueous lithium–oxygen batteries, and a favourable catalytic effect on Li_2O_2 formation and decomposition was found. In a similar manner, Er-CeO_2 was loaded onto graphene oxide directly via in situ hydrothermal crystallisation, and then in a second hydrothermal step, CuO was co-loaded; these composite materials showed enhanced photocatalytic reduction of CO_2 to methanol compared to the individual components [163]. Xu et al. used polystyrene microspheres as templates to produce hollow microspheres constructed from agglomerated crystallites of Y-substituted CeO_2: these showed enhanced activity for the photocatalytic decomposition of acetaldehyde [158].

3.5. Multi-Element Substitutions

Given the wide range of chemical elements that can easily be added to ceria using the very mild conditions offered by solvothermal approaches, it is not surprising to find that multi-element inclusion has been increasingly explored as a way of fine-tuning properties such as oxygen storage or photocatalysis and perhaps also introducing the possibility of multifunctionality in the solid materials. This includes combining elements of similar chemistry that might provide some cooperative effect on resulting properties, such as more than one of the rare earths [164–168]. Mixing elements from different parts of the periodic table is also increasingly being explored, and one important example is the inclusion of other rare earths in ceria-zirconia solid solutions that may further tune redox properties for heterogeneous catalysis. For example, by addition of both Zr and Pr to ceria, via a hydrothermal route, it was shown that praseodymium contributes positively towards the soot oxidation reaction, but it has an adverse effect on CO oxidation over the same catalysts, as compared to pure ceria [169]. The inclusion of both Nd and La to ceria-zirconia, to give a phase with 40% cerium, 50% zirconium, 5% lanthanum and 5% neodymium, via a mild hydrothermal crystallisation, gave materials with enhanced low-temperature reducibility and thermal stability [170]. Materials in the CeO_2-Y_2O_3-ZrO_2 system have been prepared under solvothermal conditions. Wang et al. found that the activation energy of crystal growth is significantly dependent on the CeO_2 concentration [171], and continuous flow synthesis (410 °C, 27 MPa) has been used to form ultrafine stabilised tetragonal zirconia particles [172], while a wide range of nanoscale crystal forms, with intricate morphologies,

were possible by inclusion of surfactants, Figure 20 [173]. In the even more complex system ceria-zirconia-yttria-lanthana, high-surface area nanostructured materials have been formed with the aid of lauric acid and dodecylamine [174].

Europium has been added to ceria-zirconia in low concentrations (<10%) using aqueous ammonia as a reaction medium and potassium oleate as an additive to produce nanocrystalline materials with photoemission and photoluminescence properties [175,176]. Hydrothermal synthesis using poly block copolymer surfactants provides high-surface La-containing ceria zirconia [177].

Mixed rare earth ceria materials with other substituents have been prepared via hydrothermal methods, such as Sr,Gd-ceria [178] and Bi,Gd-ceria [179,180], and sintered into ceramics for solid oxide fuel cell applications.

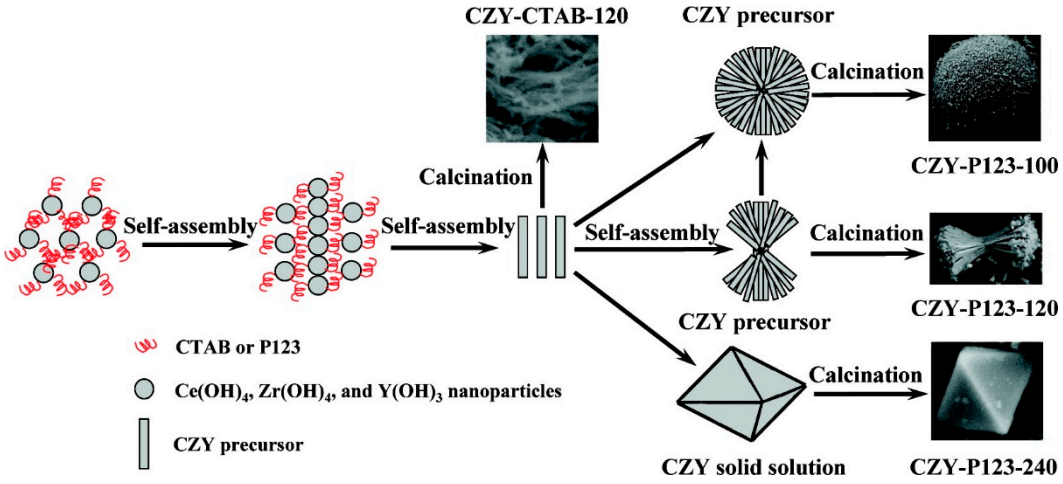

Figure 20. A schematic illustration of formation mechanisms of the ceria-zirconia-yttria precursors and ceria-zirconia-yttria solid solutions under surfactant-assisted (CTAB or P123) hydrothermal and calcination conditions [173]. Reprinted with permission from Zhang, Y.; Zhang, L.; Deng, J.; Dai, H.; He, H. Controlled Synthesis, Characterization, and Morphology-Dependent Reducibility of Ceria−Zirconia−Yttria Solid Solutions with Nanorod-like, Microspherical, Microbowknot-like, and Micro-octahedral Shapes. *Inorg. Chem.* **2009**, *48*, 2181–2192. Copyright (2009) American Chemical Society.

4. Summary, Challenges and Future Directions

Our survey of the past decade of research on solvothermal synthesis methods for producing cerium dioxide materials has shown how elements from every part of the periodic table can be introduced into the cubic fluorite lattice of CeO_2. Our earlier review 10 years ago found relatively few examples of substitutional chemistry, with the main emphasis being on ceria-zirconia solid solutions and rare-earth substituents, in all cases using water as the majority solvent [30]. This work has now been broadened to encompass an extensive set of element substitutions, including mixtures of elements, and using a variety of solvents, solvent mixtures and solution additives. As with other oxide materials, the advantage of the solvothermal method lies in the accessing of novel substitutional chemistry and in the control of crystal form, both of which are difficult when higher temperatures are employed, such as in classical solid-state chemistry, or combustion methods, or even in simple precipitation routes that require a firing step to induce crystallisation [181]. The solvothermal synthesis method typically yields materials in a crystalline state, even if a mild heat treatment (up to 500 °C) may be used to remove any surface-bound hydroxide, solvent or additive, particularly when the materials are to be used for applications in heterogeneous catalysis. Much of the research reported is towards practical applications and as well as classical fields of research, such as in redox catalysis, photocatalysis and oxide ion conductivity, novel directions are being explored and, indeed, enabled by the availability of nanocrystalline forms of ceria. This includes applications as components in solar devices, as electrodes in rechargeable batteries and as catalysts for thermochemical

water splitting and has allowed properties such as luminescent sensing, magnetism and toxicity to be studied.

The nanoscale crystal morphologies are important where high surface areas are needed but also provide highly sinterable powders for forming ceramics, such as electrodes for solid oxide fuel cells. In this respect, it is important to consider the level of control over crystal morphology under solvothermal reaction conditions and whether this has truly been demonstrated with any degree of predictability. As this review has shown, a wide variety of solution additives and solvents have now been employed, and, certainly, in some cases, enough examples are provided, independently by different research groups, to identify certain conditions that yield specific crystal morphologies. For example, $Na_3PO_4{\cdot}12H_2O$ has been used to form octahedral-shaped crystals for CeO_2 itself, as well as for various substituted versions. However, the mechanism of its action has not been uncovered, beyond speculation of control of the solution pH. The formation of nanorod morphologies is often related to the formation of lanthanide trihydroxides, implying either a seeding effect of $Ln(OH)_3$ which forms early in the synthesis, or thermal decomposition yielding oxides with morphological control. In many cases, the role of the solution additives (along with the choice of solvent) is unknown and many authors reported the outcome of the use of the additive without any consideration of its role.

From our review, three trends are emerging in tuning the properties of materials for applications which make use of the full advantages of solvothermal chemistry, and these are ripe for future development.

(1) Multi-element substitution is now increasingly being used to adjust properties, and this has been extended from mixtures of rare-earth substituents to combinations of, for example, rare earths in ceria-zirconia to mixtures of transition metal ions. This includes compositions that might be expected to phase separate in alternative synthesis approaches, particularly those that use an annealing to induce crystallisation. Here, computer simulation, which has long been used to understand the effect of M^{3+} substituents in ceria [182], may provide important guiding principles in narrowing down likely candidate combinations of substituting elements.

(2) The formation of composite materials is being tuned to introduce dual functionality or enhanced properties beyond the individual components: this includes the purposeful growth of mixed-phase materials where one oxide is grown in intimate proximity to a second. This may give interesting properties from the interfaces present between the two phases but may also yield morphologies not possible by other routes, and the example of CeO_2-CuO illustrates this.

(3) The use of in situ growth on templates or substrates allows fabrication of materials in a form suited for application. For example, impregnation of a porous support material with a reagent solution, followed by hydrothermal crystallisation, provides a convenient method for the formation of a device, and an example of ceria nanorods grown within a ceramic matrix for an electrode in solid oxide fuel cells illustrates this concept. The same idea could be used to produce coating or films of an immobilised material. This is of importance in emerging applications of ceria materials, such as in electrocatalysis, where the role of a support is crucial to determine properties [183].

In consideration of the directed synthesis of active materials for applications, there are some outstanding issues that are apparent from the literature we have reviewed:

(1) A detailed atomic-scale characterisation of materials is needed to understand fully structure–property relationships to then justify and predict choices of elemental substitution. The vast majority of work reviewed above has relied on the use of powder X-ray diffraction patterns and electron microscopy to prove sample identity and purity, in some cases supplemented by Raman spectroscopy as an additional fingerprint. Very few works have performed an in-depth analysis of the local atomic structure in the substituted materials, which is likely to be highly distorted from the ideal fluorite structure, when the coordination preferences of cations are taken into consideration: for example, the Jahn–Teller distortion expected for Cu^{2+}, or the asymmetric environment expected for Bi^{3+}

in an oxide. In multi-element substitutions, the issue of local atomic clustering, i.e., the homogeneity of element mixing, must be considered. Even for the case where an isovalent substitution is made, such as in ceria-zirconia solid solutions, there are complex structure–composition phase diagrams, and nanoscale phase segregation is possible. Here, methods such as EXAFS spectroscopy and pair distribution function analysis must be employed to determine these structural subtleties that are hidden in conventional diffraction measurements, especially when powder diffraction profiles are broadened by a small crystallite domain size.

(2) Crystallisation mechanisms, including the mode of operation of crystal habit modifiers mentioned above, must be understood in order to plan synthesis effectively and to develop tailored synthesis to target materials with a desired structure and properties. The use of high-energy X-rays has proved highly beneficial in this respect to track the evolution of a crystalline material from within a realistic reaction vessel as a function of temperature and time [96]. This yields quantitative kinetic information and also the possibility of observation of any intermediate phases, and an example of such a study of Bi-CeO_2 is provided above. If pair distribution functions can be measured in situ, then this provides local structure information, without the requirement for a crystalline structure, and such an approach has already been applied for CeO_2 itself where nucleation was observed from previously unknown cerium dimer complexes [184]. The more widespread use of such methods will lead to the mechanistic detail needed for predictive synthesis, and this will include a proper understanding of the role of additives in modifying crystal habit. Computer simulation may also play a part in such efforts.

(3) Scale-up of synthesis for applications is crucial if materials' properties are to be put into real use. As was highlighted above several times, the use of continuous flow reactors has been the focus of development for a number of years, where a flow of reagents is rapidly mixed with a heated solvent, often under supercritical conditions, to give rapid nucleation and an output stream of a slurry of a product. This has already been put to use on a commercial scale, and cerium oxide products are available commercially [185]. Much more development needs to be conducted on developing scaled synthesis when the use of additives and crystal habit modifiers is used, and with the much more complex chemical compositions that are now being investigated; here, mixing and inclusion of additives must be carefully considered.

(4) The choice of precursors in the preparation of any functional material is of crucial importance since contaminant ions can modify the properties of the solid. In the case of ceria, alkali metal cations can act as a poison when used in selective catalytic oxidation of NO_x or NH_3 [186,187]. On the other hand, the presence of sodium can have a beneficial effect in other applications; for example, it can act as a promoter when ceria is used for ethane oxidation [188], and its inclusion in ceria-zirconia can lead to enhanced low-temperature reproducibility [189]. Similarly, chloride ions can influence the surface properties of ceria, in some cases enhancing interaction with supported species [190], while in others having a detrimental effect by the formation of CeOCl that results in loss of surface area [191]. It is also the case that the choice of precipitant can affect the sintering behaviour of ceria powders [192]. In an industrial setting, extensive washing of powders must be avoided, and therefore to achieve reproducibility in the properties of ceria materials prepared from solution, future work must consider the role of surface contaminants that arise from the choice of chemical reagents; this is true whether the contaminants have a detrimental or a beneficial effect.

(5) The toxicity of nanocrystals to humans and other organisms is a growing concern, and ceria has attracted some attention in this respect, especially given its biological activity arising from its antioxidant properties. With a growing range of specimens available from solvothermal chemistry, each with their own distinctive chemistry from the substituent cations, clearly consideration of biotoxicity must be the focus of greater attention. As well as studies of the action of nanoparticles in biological systems, their transport into the human body is another important field of research, whether by inhalation or through the

skin. This has recently been examined for CeO_2 itself [193], but there is much further work to be conducted in this respect.

Finally, we note that in the case of CeO_2 itself, a recent article by Xu et al. extensively reviewed the various solution methods for synthesis, including solvothermal methods, and attempted to classify the various influences on crystal growth with the aim of having some predictability in the control of the crystal form, Figure 21 [194]. While the addition of a substituting cation, and indeed habit-modifying additives, introduces further complexity, it is highly likely that the same principles put forward will apply to the wider family of cerium oxide materials. This accumulation of experimental evidence leads to the possibility of controlled synthesis of materials with highly tuned properties for applications.

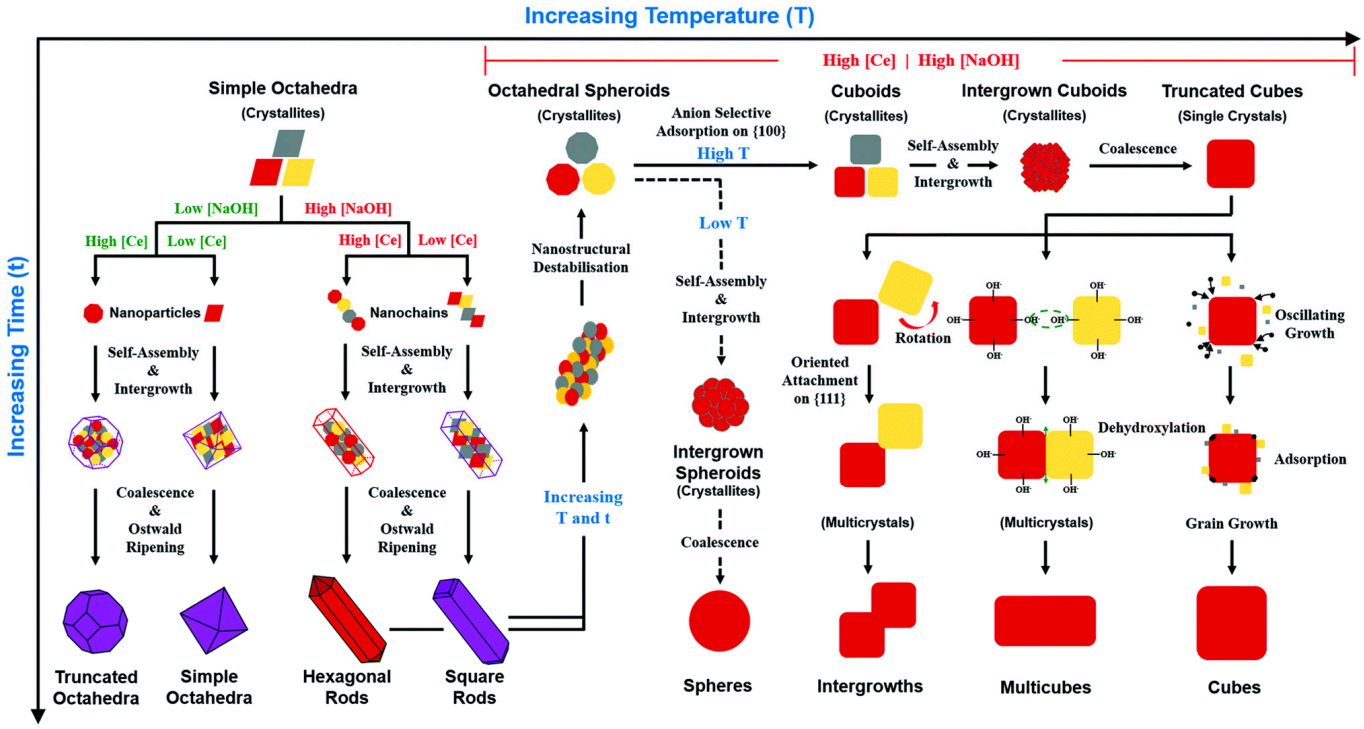

Figure 21. Schematic of solution growth mechanisms of CeO_{2-x} nanomorphologies (red/yellow = investigated by Xu et al. [194]; purple = from the literature; [Ce]: low < 0.50 M ≤ high; [NaOH]: low < 5.00 M ≤ high; *T*: low < 150 °C ≤ high; *t*: short ≤ 2 h < long) [194]. Reproduced from Xu, Y.; Mofarah, S.S.; Mehmood, R.; Cazorla, C.; Koshy, P.; Sorrell, C.C. Design strategies for ceria nanomaterials: untangling key mechanistic concepts. *Mater. Horiz.* **2021**, *8*, 102–123—Published by The Royal Society of Chemistry.

5. Conclusions

Solvothermal synthesis routes to substituted cerium oxides provide versatile conditions for the preparation and, ultimately, manufacture of functional materials for use in established and emerging applications. The accumulated literature points towards a move to control of the chemical composition and crystal form, with particular emphasis on the nanostructure. We have emphasised developing trends in targeting complex compositions with multi-element replacements, and in the preparation of composite phases, including in situ growth onto substrates to fabricate devices for application. There are also a number of challenges in developing future targeted synthesis of novel materials, which include more in-depth structural characterisation of existing materials to provide proper structure–property relationships, and in situ studies of crystallisation to provide the formation mechanism with a firmer basis. Finally, scale-up of synthesis requires further consideration, bearing in mind the complex mixtures of reagents being used to tailor the crystal form.

Supplementary Materials: The following are available online at https://www.mdpi.com/article/10.3390/inorganics9060040/s1. Table S1: Summary of rare-earth substituted cerium dioxide materials prepared by solvothermal synthesis. Please see Supplementary File.

Author Contributions: Conceptualization, J.M.F., D.T., R.I.W.; writing—original draft preparation, J.W.A., R.I.W.; writing—reviewing and editing, J.W.A., R.I.W.; funding acquisition, R.I.W. All authors have read and agreed to the published version of the manuscript.

Funding: This work was supported by the Royal Society via PhD position for J.W.A. and an Industry Fellowship in collaboration with Johnson Matthey for R.I.W.

Institutional Review Board Statement: Not applicable.

Informed Consent Statement: Not applicable.

Data Availability Statement: Data sharing not applicable.

Acknowledgments: The authors acknowledge the financial support of the Royal Society.

Conflicts of Interest: The authors declare no conflict of interest.

References

1. Trovarelli, A. Catalytic properties of ceria and CeO_2-containing materials. *Catal. Rev. Sci. Eng.* **1996**, *38*, 439–520. [CrossRef]
2. Montini, T.; Melchionna, M.; Monai, M.; Fornasiero, P. Fundamentals and Catalytic Applications of CeO_2-Based Materials. *Chem. Rev.* **2016**, *116*, 5987–6041. [CrossRef] [PubMed]
3. Kim, G. Ceria-promoted three-way catalysts for auto exhaust emission control. *Ind. Eng. Chem. Prod. Res. Dev.* **1982**, *21*, 267–274. [CrossRef]
4. Diwell, A.F.; Rajaram, R.R.; Shaw, H.A.; Truex, T.J. The Role of Ceria in Three-Way Catalysts. In *Studies in Surface Science and Catalysis*; Crucq, A., Ed.; Elsevier: Amsterdam, The Netherlands, 1991; Volume 71, pp. 139–152.
5. Li, P.; Chen, X.; Li, Y.; Schwank, J.W. A review on oxygen storage capacity of CeO_2-based materials: Influence factors, measurement techniques, and applications in reactions related to catalytic automotive emissions control. *Catal. Today* **2019**, *327*, 90–115. [CrossRef]
6. Soykal, I.I.; Sohn, H.; Singh, D.; Miller, J.T.; Ozkan, U.S. Reduction Characteristics of Ceria under Ethanol Steam Reforming Conditions: Effect of the Particle Size. *ACS Catal.* **2014**, *4*, 585–592. [CrossRef]
7. Liu, S.; Wu, X.; Weng, D.; Ran, R. Ceria-based catalysts for soot oxidation: A review. *J. Rare Earths* **2015**, *33*, 567–590. [CrossRef]
8. Gorte, R.J.; Zhao, S. Studies of the water-gas-shift reaction with ceria-supported precious metals. *Catal. Today* **2005**, *104*, 18–24. [CrossRef]
9. Wang, Q.; Yeung, K.L.; Bañares, M.A. Ceria and its related materials for VOC catalytic combustion: A review. *Catal. Today* **2020**, *356*, 141–154. [CrossRef]
10. Le Gal, A.; Abanades, S.; Bion, N.; Le Mercier, T.; Harlé, V. Reactivity of Doped Ceria-Based Mixed Oxides for Solar Thermochemical Hydrogen Generation via Two-Step Water-Splitting Cycles. *Energy Fuels* **2013**, *27*, 6068–6078. [CrossRef]
11. Jaiswal, N.; Tanwar, K.; Suman, R.; Kumar, D.; Upadhyay, S.; Parkash, O. A brief review on ceria based solid electrolytes for solid oxide fuel cells. *J. Alloys Compd.* **2019**, *781*, 984–1005. [CrossRef]
12. Shcherbakov, A.B.; Ivanov, V.K.; Zholobak, N.M.; Ivanova, O.S.; Krysanov, E.Y.; Baranchikov, A.E.; Spivak, N.Y.; Tretyakov, Y.D. Nanocrystalline ceria based materials—Perspectives for biomedical application. *Biophysics* **2011**, *56*, 987–1004. [CrossRef]
13. Xu, C.; Qu, X.G. Cerium oxide nanoparticle: A remarkably versatile rare earth nanomaterial for biological applications. *NPG Asia Mater.* **2014**, *6*, e90. [CrossRef]
14. Casals, E.; Zeng, M.; Parra-Robert, M.; Fernández-Varo, G.; Morales-Ruiz, M.; Jiménez, W.; Puntes, V.; Casals, G. Cerium Oxide Nanoparticles: Advances in Biodistribution, Toxicity, and Preclinical Exploration. *Small* **2020**, *16*, 1907322. [CrossRef] [PubMed]
15. Yabe, S.; Yamashita, M.; Momose, S.; Tahira, K.; Yoshida, S.; Li, R.; Yin, S.; Sato, T. Synthesis and UV-shielding properties of metal oxide doped ceria via soft solution chemical processes. *Int. J. Inorg. Mater.* **2001**, *3*, 1003–1008. [CrossRef]
16. Yabe, S.; Sato, T. Cerium oxide for sunscreen cosmetics. *J. Solid State Chem.* **2003**, *171*, 7–11. [CrossRef]
17. Caputo, F.; De Nicola, M.; Sienkiewicz, A.; Giovanetti, A.; Bejarano, I.; Licoccia, S.; Traversa, E.; Ghibelli, L. Cerium oxide nanoparticles, combining antioxidant and UV shielding properties, prevent UV-induced cell damage and mutagenesis. *Nanoscale* **2015**, *7*, 15643–15656. [CrossRef]
18. Feng, X.; Sayle, D.C.; Wang, Z.L.; Paras, M.S.; Santora, B.; Sutorik, A.C.; Sayle, T.X.T.; Yang, Y.; Ding, Y.; Wang, X.; et al. Converting ceria polyhedral nanoparticles into single-crystal nanospheres. *Science* **2006**, *312*, 1504–1508. [CrossRef] [PubMed]
19. Fu, X.Q.; Wang, C.; Yu, H.C.; Wang, Y.G.; Wang, T.H. Fast humidity sensors based on CeO_2 nanowires. *Nanotechnology* **2007**, *18*, 145503. [CrossRef]
20. Schmitt, R.; Nenning, A.; Kraynis, O.; Korobko, R.; Frenkel, A.I.; Lubomirsky, I.; Haile, S.M.; Rupp, J.L.M. A review of defect structure and chemistry in ceria and its solid solutions. *Chem. Soc. Rev.* **2020**, *49*, 554–592. [CrossRef]
21. Di Monte, R.; Kašpar, J. Heterogeneous environmental catalysis—A gentle art: CeO_2–ZrO_2 mixed oxides as a case history. *Catal. Today* **2005**, *100*, 27–35. [CrossRef]

22. Gao, Y.X.; Wang, W.D.; Chang, S.J.; Huang, W.X. Morphology Effect of CeO_2 Support in the Preparation, Metal-Support Interaction, and Catalytic Performance of Pt/CeO_2 Catalysts. *Chemcatchem* **2013**, *5*, 3610–3620. [CrossRef]
23. Qiao, Z.A.; Wu, Z.L.; Dai, S. Shape-Controlled Ceria-based Nanostructures for Catalysis Applications. *ChemSusChem* **2013**, *6*, 1821–1833. [CrossRef] [PubMed]
24. Wang, S.; Zhao, L.; Wang, W.; Zhao, Y.; Zhang, G.; Ma, X.; Gong, J. Morphology control of ceria nanocrystals for catalytic conversion of CO_2 with methanol. *Nanoscale* **2013**, *5*, 5582–5588. [CrossRef] [PubMed]
25. Aneggi, E.; Wiater, D.; de Leitenburg, C.; Llorca, J.; Trovarelli, A. Shape-Dependent Activity of Ceria in Soot Combustion. *ACS Catal.* **2014**, *4*, 172–181. [CrossRef]
26. Trovarelli, A.; Llorca, J. Ceria Catalysts at Nanoscale: How Do Crystal Shapes Shape Catalysis? *ACS Catal.* **2017**, *7*, 4716–4735. [CrossRef]
27. Kašpar, J.; Di Monte, R.; Fornasiero, P.; Graziani, M.; Bradshaw, H.; Norman, C. Dependency of the Oxygen Storage Capacity in Zirconia–Ceria Solid Solutions upon Textural Properties. *Top. Catal.* **2001**, *16*, 83–87. [CrossRef]
28. Monte, R.D.; Kašpar, J. Nanostructured CeO_2–ZrO_2 mixed oxides. *J. Mater. Chem.* **2005**, *15*, 633–648. [CrossRef]
29. Sun, C.; Li, H.; Chen, L. Nanostructured ceria-based materials: Synthesis, properties, and applications. *Energy Environ. Sci.* **2012**, *5*, 8475–8505. [CrossRef]
30. Walton, R.I. Solvothermal synthesis of cerium oxides. *Prog. Cryst. Growth Charact. Mater.* **2011**, *57*, 93–108. [CrossRef]
31. Rabenau, A. The Role of Hydrothermal Synthesis in Preparative Chemistry. *Angew. Chem. Int. Ed.* **1985**, *24*, 1026–1040. [CrossRef]
32. Yoshimura, M.; Byrappa, K. Hydrothermal processing of materials: Past, present and future. *J. Mater. Sci.* **2008**, *43*, 2085–2103. [CrossRef]
33. Cundy, C.S.; Cox, P.A. The hydrothermal synthesis of zeolites: History and development from the earliest days to the present time. *Chem. Rev.* **2003**, *103*, 663–701. [CrossRef] [PubMed]
34. Laudise, R.A. Hydrothermal Synthesis of Crystals. *Chem. Eng. News* **1987**, *65*, 30–43. [CrossRef]
35. Demazeau, G. Solvothermal reactions: An original route for the synthesis of novel materials. *J. Mater. Sci.* **2008**, *43*, 2104–2114. [CrossRef]
36. Sōmiya, S.; Roy, R. Hydrothermal synthesis of fine oxide powders. *Bull. Mater. Sci.* **2000**, *23*, 453–460. [CrossRef]
37. Riman, R.E.; Suchanek, W.L.; Lencka, M.M. Hydrothermal crystallization of ceramics. *Ann. Chim. Sci. Mater.* **2002**, *27*, 15–36. [CrossRef]
38. Walton, R.I. Subcritical solvothermal synthesis of condensed inorganic materials. *Chem. Soc. Rev.* **2002**, *31*, 230–238. [CrossRef]
39. Komarneni, S. Nanophase materials by hydrothermal, microwave-hydrothermal and microwave-solvothermal methods. *Curr. Sci.* **2003**, *85*, 1730–1734.
40. Kumada, N. Preparation and crystal structure of new inorganic compounds by hydrothermal reaction. *J. Ceram. Soc. Jpn.* **2013**, *121*, 135–141. [CrossRef]
41. Tani, E.; Yoshimura, M.; Sōmiya, S. Crystallization and crystal growth of CeO_2 under hydrothermal conditions. *J. Mater. Sci. Lett.* **1982**, *1*, 461–462. [CrossRef]
42. Montini, T.; Speghini, A.; Rogatis, L.D.; Lorenzut, B.; Bettinelli, M.; Graziani, M.; Fornasiero, P. Identification of the Structural Phases of $Ce_xZr_{1-x}O_2$ by Eu(III) Luminescence Studies. *J. Am. Chem. Soc.* **2009**, *131*, 13155–13160. [CrossRef]
43. Yang, Z.; Hu, W.; Zhang, N.; Li, Y.; Liao, Y. Facile synthesis of ceria–zirconia solid solutions with cubic–tetragonal interfaces and their enhanced catalytic performance in diesel soot oxidation. *J. Catal.* **2019**, *377*, 98–109. [CrossRef]
44. Luciani, G.; Landi, G.; Imparato, C.; Vitiello, G.; Deorsola, F.A.; Di Benedetto, A.; Aronne, A. Improvement of splitting performance of $Ce_{0.75}Zr_{0.25}O_2$ material: Tuning bulk and surface properties by hydrothermal synthesis. *Int. J. Hydrogen Energy* **2019**, *44*, 17565–17577. [CrossRef]
45. Wang, H.; Yang, G.-Q.; Song, Y.-H.; Liu, Z.-T.; Liu, Z.-W. Defect-rich $Ce_{1-x}Zr_xO_2$ solid solutions for oxidative dehydrogenation of ethylbenzene with CO_2. *Catal. Today* **2019**, *324*, 39–48. [CrossRef]
46. Wan, J.; Lin, J.; Guo, X.; Wang, T.; Zhou, R. Morphology effect on the structure-activity relationship of Rh/CeO_2-ZrO_2 catalysts. *Chem. Eng. J.* **2019**, *368*, 719–729. [CrossRef]
47. Liu, X.; Liu, W.; Zhang, X.; Han, L.; Zhang, C.; Yang, Y. Zr-doped CeO_2 Hollow slightly-truncated nano-octahedrons: One-pot synthesis, characterization and their application in catalysis of CO oxidation. *Cryst. Res. Technol.* **2014**, *49*, 383–392. [CrossRef]
48. Chen, A.; Zhou, Y.; Ta, N.; Li, Y.; Shen, W. Redox properties and catalytic performance of ceria–zirconia nanorods. *Catal. Sci. Technol.* **2015**, *5*, 4184–4192. [CrossRef]
49. Wang, R.; Mutinda, S.I.; Fang, M. One-pot hydrothermal synthesis and high temperature thermal stability of $Ce_xZr_{1-x}O_2$ nanocrystals. *RSC Adv.* **2013**, *3*, 19508–19514. [CrossRef]
50. Das, S.; Gupta, R.; Kumar, A.; Shah, M.; Sengupta, M.; Bhandari, S.; Bordoloi, A. Facile Synthesis of Ruthenium Decorated $Zr_{0.5}Ce_{0.5}O_2$ Nanorods for Catalytic Partial Oxidation of Methane. *ACS Appl. Nano Mater.* **2018**, *1*, 2953–2961. [CrossRef]
51. Kim, J.-R.; Myeong, W.-J.; Ihm, S.-K. Characteristics in oxygen storage capacity of ceria–zirconia mixed oxides prepared by continuous hydrothermal synthesis in supercritical water. *Appl. Catal. B Environ.* **2007**, *71*, 57–63. [CrossRef]
52. Kim, J.-R.; Lee, K.-Y.; Suh, M.-J.; Ihm, S.-K. Ceria–zirconia mixed oxide prepared by continuous hydrothermal synthesis in supercritical water as catalyst support. *Catal. Today* **2012**, *185*, 25–34. [CrossRef]

53. Auxéméry, A.; Frias, B.B.; Smal, E.; Dziadek, K.; Philippot, G.; Legutko, P.; Simonov, M.; Thomas, S.; Adamski, A.; Sadykov, V.; et al. Continuous supercritical solvothermal preparation of nanostructured ceria-zirconia as supports for dry methane reforming catalysts. *J. Supercrit. Fluids* **2020**, *162*, 104855. [CrossRef]
54. Tang, X.; Zhang, B.; Li, Y.; Xu, Y.; Xin, Q.; Shen, W. CuO/CeO_2 catalysts: Redox features and catalytic behaviors. *Appl. Catal. A Gen.* **2005**, *288*, 116–125. [CrossRef]
55. Bernardi, M.I.B.; Mesquita, A.; Béron, F.; Pirota, K.R.; De Zevallos, A.O.; Doriguetto, A.C.; De Carvalho, H.B. The role of oxygen vacancies and their location in the magnetic properties of $Ce_{1-x}Cu_xO_{2-\delta}$ nanorods. *Phys. Chem. Chem. Phys.* **2015**, *17*, 3072–3080. [CrossRef]
56. Wang, J.; Liu, Q.; Liu, Q. Ceria- and Cu-doped ceria nanocrystals synthesized by the hydrothermal methods. *J. Am. Ceram. Soc.* **2008**, *91*, 2706–2708. [CrossRef]
57. Yang, F.; Wei, J.; Liu, W.; Guo, J.; Yang, Y. Copper doped ceria nanospheres: Surface defects promoted catalytic activity and a versatile approach. *J. Mater. Chem. A* **2014**, *2*, 5662–5667. [CrossRef]
58. Yang, H.; Pan, Y.; Xu, Y.; Yang, Y.; Sun, G. Enhanced catalytic performance of $(CuO)_x/Ce_{0.9}Cu_{0.1}O_2$ nanospheres: Combined contribution of the synergistic effect and surface defects. *ChemPlusChem* **2015**, *80*, 886–894. [CrossRef]
59. Rood, S.C.; Pastor-Algaba, O.; Tosca-Princep, A.; Pinho, B.; Isaacs, M.; Torrente-Murciano, L.; Eslava, S. Synergistic Effect of Simultaneous Doping of Ceria Nanorods with Cu and Cr on CO Oxidation and NO Reduction. *Chem. Eur. J.* **2021**, *27*, 2165–2174. [CrossRef]
60. Zhang, J.; Guo, J.; Liu, W.; Wang, S.; Xie, A.; Liu, X.; Wang, J.; Yang, Y. Facile preparation of Mn^{n+}-Doped (M = Cu, Co, Ni, Mn) hierarchically mesoporous CeO_2 nanoparticles with enhanced catalytic activity for CO oxidation. *Eur. J. Inorg. Chem.* **2015**, *2015*, 969–976. [CrossRef]
61. Kurajica, S.; Mužina, K.; Dražić, G.; Matijašić, G.; Duplančić, M.; Mandić, V.; Župančić, M.; Munda, I.K. A comparative study of hydrothermally derived Mn, Fe, Co, Ni, Cu and Zn doped ceria nanocatalysts. *Mater. Chem. Phys.* **2020**, *244*, 122689. [CrossRef]
62. Syed Khadar, Y.A.; Balamurugan, A.; Devarajan, V.P.; Subramanian, R.; Dinesh Kumar, S. Synthesis, characterization and antibacterial activity of cobalt doped cerium oxide (CeO_2:Co) nanoparticles by using hydrothermal method. *J. Mater. Res.* **2019**, *8*, 267–274. [CrossRef]
63. Zhang, X.; Wei, J.; Yang, H.; Liu, X.; Liu, W.; Zhang, C.; Yang, Y. One-Pot Synthesis of Mn-Doped CeO_2 Nanospheres for CO Oxidation. *Eur. J. Inorg. Chem.* **2013**, *2013*, 4443–4449. [CrossRef]
64. Zhang, Y.; Yang, F.; Gao, R.; Dai, W.L. Manganese-doped CeO_2 nanocubes as highly efficient catalysts for styrene epoxidation with TBHP. *App.Surf. Sci.* **2019**, *471*, 767–775.
65. Jampaiah, D.; Venkataswamy, P.; Coyle, V.E.; Reddy, B.M.; Bhargava, S.K. Low-temperature CO oxidation over manganese, cobalt, and nickel doped CeO_2 nanorods. *RSC Adv.* **2016**, *6*, 80541–80548. [CrossRef]
66. Song, Q.; Ran, R.; Ding, J.; Wu, X.; Si, Z.; Weng, D. The controlled preparation and performance of Fe, Co-modified porous ceria nanorods for the total oxidation of propane. *Mol. Catal.* **2020**, *480*, 110663. [CrossRef]
67. Xing, X.; Cai, Y.; Chen, N.; Li, Y.; Deng, D.; Wang, Y. Synthesis of mixed Mn–Ce–O_x one dimensional nanostructures and their catalytic activity for CO oxidation. *Ceram. Int.* **2015**, *41*, 4675–4682. [CrossRef]
68. Liu, X.; Han, L.; Liu, W.; Yang, Y. Synthesis of Co/Ni unitary- or binary-doped CeO_2 mesoporous nanospheres and their catalytic performance for CO oxidation. *Eur. J. Inorg. Chem.* **2014**, *2014*, 5370–5377.
69. Du, X.; Dai, Q.; Wei, Q.; Huang, Y. Nanosheets-assembled Ni (Co) doped CeO_2 microspheres toward NO + CO reaction. *Appl. Catal. A Gen.* **2020**, *602*, 117728. [CrossRef]
70. Venkataswamy, P.; Damma, D.; Jampaiah, D.; Mukherjee, D.; Vithal, M.; Reddy, B.M. Cr-Doped CeO_2 Nanorods for CO Oxidation: Insights into Promotional Effect of Cr on Structure and Catalytic Performance. *Catal. Lett.* **2020**, *150*, 948–962.
71. Phokha, S.; Pinitsoontorn, S.; Maensiri, S. Structure and Magnetic Properties of Monodisperse Fe3+-doped CeO2 Nanospheres. *Nano-Micro Lett.* **2013**, *3*, 223–233.
72. Wang, W.; Zhu, Q.; Qin, F.; Dai, Q.; Wang, X. Fe doped CeO_2 nanosheets as Fenton-like heterogeneous catalysts for degradation of salicylic acid. *Chem. Eng. J.* **2018**, *333*, 226–239. [CrossRef]
73. Zheng, X.; Li, Y.; Zheng, Y.; Shen, L.; Xiao, Y.; Cao, Y.; Zhang, Y.; Au, C.; Jiang, L. Highly Efficient Porous $Fe_xCe_{1-x}O_{2-\delta}$ with Three-Dimensional Hierarchical Nanoflower Morphology for H_2S-Selective Oxidation. *ACS Catal.* **2020**, *10*, 3968–3983. [CrossRef]
74. Liu, W.; Wang, W.; Tang, K.; Guo, J.; Ren, Y.; Wang, S.; Feng, L.; Yang, Y. The promoting influence of nickel species in the controllable synthesis and catalytic properties of nickel–ceria catalysts. *Catal. Sci. Tech.* **2016**, *6*, 2427–2434. [CrossRef]
75. Tsoncheva, T.; Rosmini, C.; Dimitrov, M.; Issa, G.; Henych, J.; Němečková, Z.; Kovacheva, D.; Velinov, N.; Atanasova, G.; Spassova, I. Formation of Catalytic Active Sites in Hydrothermally Obtained Binary Ceria–Iron Oxides: Composition and Preparation Effects. *ACS Appl. Mater. Inter.* **2021**, *13*, 1838–1852. [CrossRef] [PubMed]
76. Barbosa, C.C.S.; Peixoto, E.B.; Jesus, A.C.B.; Jesus, J.R.; Fabian, F.A.; Costa, I.M.; Almeida, J.M.A.; Duque, J.G.S.; Meneses, C.T. Effect of doping in $Ce_{1-x}TM_xO_2$ (TM = Mn, Cr, Co and Fe) nanoparticles obtained by hydrothermal method. *Mater. Chem. Phys.* **2019**, *225*, 187–191. [CrossRef]
77. Radović, M.; Dohčević-Mitrović, Z.; Golubović, A.; Fruth, V.; Preda, S.; Šćepanović, M.; Popović, Z.V. Influence of Fe^{3+}-doping on optical properties of CeO_{2-y} nanopowders. *Ceram. Int.* **2013**, *39*, 4929–4936. [CrossRef]
78. Chen, X.; Zhan, S.; Chen, D.; He, C.; Tian, S.; Xiong, Y. Grey Fe-$CeO_{2-\sigma}$ for boosting photocatalytic ozonation of refractory pollutants: Roles of surface and bulk oxygen vacancies. *Appl. Catal. B Environ.* **2021**, *286*, 119928. [CrossRef]

79. Ma, Y.; Ma, Y.; Giuli, G.; Euchner, H.; Groß, A.; Lepore, G.O.; d'Acapito, F.; Geiger, D.; Biskupek, J.; Kaiser, U.; et al. Introducing Highly Redox-Active Atomic Centers into Insertion-Type Electrodes for Lithium-Ion Batteries. *Adv. Ener. Mater.* **2020**, *10*, 2000783. [CrossRef]
80. Zhang, G.; Li, Y.; Zhao, X.; Xu, J.; Zhang, Y. The variation of microstructures, spectral characteristics and catalysis effects of Fe^{3+} and Zn^{2+} co-doped CeO_2 solid solutions. *J. Rare Earths* **2020**, *38*, 241–249. [CrossRef]
81. Dosa, M.; Piumetti, M.; Bensaid, S.; Andana, T.; Novara, C.; Giorgis, F.; Fino, D.; Russo, N. Novel Mn–Cu-Containing CeO_2 Nanopolyhedra for the Oxidation of CO and Diesel Soot: Effect of Dopants on the Nanostructure and Catalytic Activity. *Catal. Lett.* **2018**, *148*, 298–311. [CrossRef]
82. Zhu, H.; Chen, Y.; Gao, Y.; Liu, W.; Wang, Z.; Cui, C.; Liu, W.; Wang, L. Catalytic oxidation of CO on mesoporous codoped ceria catalysts: Insights into correlation of physicochemical property and catalytic activity. *J. Rare Earths* **2019**, *37*, 961–969. [CrossRef]
83. Ji, Y.; Jin, Z.; Li, J.; Zhang, Y.; Liu, H.; Shi, L.; Zhong, Z.; Su, F. Rambutan-like hierarchically heterostructured CeO_2-CuO hollow microspheres: Facile hydrothermal synthesis and applications. *Nano Res.* **2017**, *10*, 381–396. [CrossRef]
84. Hiley, C.I.; Fisher, J.M.; Thompsett, D.; Kashtiban, R.J.; Sloan, J.; Walton, R.I. Incorporation of square-planar Pd^{2+} in fluorite CeO_2: Hydrothermal preparation, local structure, redox properties and stability. *J. Mater. Chem. A* **2015**, *3*, 13072–13079. [CrossRef]
85. Hiley, C.I.; Playford, H.Y.; Fisher, J.M.; Felix, N.C.; Thompsett, D.; Kashtiban, R.J.; Walton, R.I. Pair Distribution Function Analysis of Structural Disorder by Nb^{5+} Inclusion in Ceria: Evidence for Enhanced Oxygen Storage Capacity from Under-Coordinated Oxide. *J. Am. Chem. Soc.* **2018**, *140*, 1588–1591. [CrossRef]
86. Ma, X.; Lu, P.; Wu, P. Structural, optical and magnetic properties of CeO_2 nanowires with nonmagnetic Mg^{2+} doping. *J. Alloys Compd.* **2018**, *734*, 22–28. [CrossRef]
87. Siqueira Júnior, J.M.; Brum Malta, L.F.; Garrido, F.M.S.; Ogasawara, T.; Medeiros, M.E. Raman and Rietveld structural characterization of sintered alkaline earth doped ceria. *Mater. Chem. Phys.* **2012**, *135*, 957–964. [CrossRef]
88. Tighe, C.J.; Cabrera, R.Q.; Gruar, R.I.; Darr, J.A. Scale Up Production of Nanoparticles: Continuous Supercritical Water Synthesis of Ce–Zn Oxides. *Ind. Eng. Chem. Res.* **2013**, *52*, 5522–5528. [CrossRef]
89. Rajkumar, T.; Sápi, A.; Ábel, M.; Kiss, J.; Szenti, I.; Baán, K.; Gómez-Pérez, J.F.; Kukovecz, Á.; Kónya, Z. Surface Engineering of CeO_2 Catalysts: Differences Between Solid Solution Based and Interfacially Designed $Ce_{1-x}M_xO_2$ and MO/CeO_2 (M = Zn, Mn) in CO_2 Hydrogenation Reaction. *Catal. Lett.* **2021**. [CrossRef]
90. Das, A.; Patra, M.; Bhagavathiachari, M.; Nair, R.G. Defect-induced visible-light-driven photocatalytic and photoelectrochemical performance of ZnO–CeO_2 nanoheterojunctions. *J. Alloys Compd.* **2021**, *858*, 157730. [CrossRef]
91. Younis, A.; Chu, D.; Kaneti, Y.V.; Li, S. Tuning the surface oxygen concentration of {111} surrounded ceria nanocrystals for enhanced photocatalytic activities. *Nanoscale* **2016**, *8*, 378–387. [CrossRef]
92. Abbas, F.; Iqbal, J.; Maqbool, Q.; Jan, T.; Ullah, M.O.; Nawaz, B. ROS mediated malignancy cure performance of morphological, optical, and electrically tuned Sn doped CeO_2 nanostructures. *AIP Adv.* **2017**, *7*, 095205. [CrossRef]
93. Shajahan, S.; Arumugam, P.; Rajendran, R.; Munusamy, A.P. Optimization and detailed stability study on Pb doped ceria nanocubes for enhanced photodegradation of several anionic and cationic organic pollutants. *Arab. J. Chem.* **2020**, *13*, 1309–1322. [CrossRef]
94. Sardar, K.; Playford, H.Y.; Darton, R.J.; Barney, E.R.; Hannon, A.C.; Tompsett, D.; Fisher, J.; Kashtiban, R.J.; Sloan, J.; Ramos, S.; et al. Nanocrystalline Cerium−Bismuth Oxides: Synthesis, Structural Characterization, and Redox Properties. *Chem. Mater.* **2010**, *22*, 6191–6201.
95. Frerichs, H.; Pütz, E.; Reich, T.; Gazanis, A.; Panthöfer, M.; Hartmann, J.; Jegel, O.; Tremel, W. Nanocomposite antimicrobials prevent bacterial growth through the enzyme-like activity of Bi-doped cerium dioxide ($Ce_{1-x}BixO_{2-\delta}$). *Nanoscale* **2020**, *12*, 21344–21358. [CrossRef]
96. Houlberg, K.; Bøjesen, E.D.; Mamakhel, A.; Wang, X.; Su, R.; Besenbacher, F.; Iversen, B.B. Hydrothermal Synthesis and in Situ Powder X-ray Diffraction Study of Bismuth-Substituted Ceria Nanoparticles. *Cryst. Growth Des.* **2015**, *15*, 3628–3636.
97. Shanavas, S.; Priyadharsan, A.; Dharmaboopathi, K. Ultrasonically and Photonically Simulatable Bi-Ceria Nanocubes for Enhanced Catalytic Degradation of Aqueous Dyes: A Detailed Study on Optimization, Mechanism and Stability. *ChemistrySelect* **2018**, *3*, 12841–12853. [CrossRef]
98. Veedu, S.N.; Jose, S.; Narendranath, S.B.; Prathapachandra Kurup, M.R.; Periyat, P. Visible light-driven photocatalytic degradation of methylene blue dye over bismuth-doped cerium oxide mesoporous nanoparticles. *Environ. Sci. Pollut. Res.* **2021**, *28*, 4147–4155. [CrossRef]
99. Hiley, C.I.; Fisher, J.M.; Kashtiban, R.J.; Cibin, G.; Thompsett, D.; Walton, R.I. Incorporation of Sb^{5+} into CeO_2: Local structural distortion of the fluorite structure from a pentavalent substituent. *Dalton Trans.* **2018**, *47*, 9693–9700.
100. Xu, Y.; Li, R. Wet-chemical synthesis and characterization of nitrogen-doped CeO_2 powders for oxygen storage capacity. *Appl. Surf. Sci.* **2018**, *455*, 997–1004. [CrossRef]
101. Liyanage, A.D.; Perera, S.D.; Tan, K.; Chabal, Y.; Balkus, K.J. Synthesis, Characterization, and Photocatalytic Activity of Y-Doped CeO_2 Nanorods. *ACS Catal.* **2014**, *4*, 577–584.
102. Mendiuk, O.; Kepinski, L. Synthesis of $Ce_{1-x}Er_xO_{2-y}$ nanoparticles by the hydrothermal method: Effect of microwave radiation on morphology and phase composition. *Ceram. Int.* **2014**, *40*, 14833–14843. [CrossRef]
103. Małecka, M.A. Characterization and thermal stability of Yb-doped ceria prepared by methods enabling control of the crystal morphology. *CrystEngComm* **2017**, *19*, 6199–6207. [CrossRef]

104. Fernandez-Garcia, S.; Jiang, L.; Tinoco, M.; Hungria, A.B.; Han, J.; Blanco, G.; Calvino, J.J.; Chen, X. Enhanced Hydroxyl Radical Scavenging Activity by Doping Lanthanum in Ceria Nanocubes. *J. Phys. Chem. C* **2016**, *120*, 1891–1901. [CrossRef]
105. Andana, T.; Piumetti, M.; Bensaid, S.; Russo, N.; Fino, D.; Pirone, R. Nanostructured ceria-praseodymia catalysts for diesel soot combustion. *Appl. Catal. B Environ.* **2016**, *197*, 125–137. [CrossRef]
106. Jiang, L.; Fernandez-Garcia, S.; Tinoco, M.; Yan, Z.; Xue, Q.; Blanco, G.; Calvino, J.J.; Hungria, A.B.; Chen, X. Improved Oxidase Mimetic Activity by Praseodymium Incorporation into Ceria Nanocubes. *ACS Appl. Mater. Inter.* **2017**, *9*, 18595–18608. [CrossRef] [PubMed]
107. Andana, T.; Piumetti, M.; Bensaid, S.; Veyre, L.; Thieuleux, C.; Russo, N.; Fino, D.; Quadrelli, E.A.; Pirone, R. Nanostructured equimolar ceria-praseodymia for NOx-assisted soot oxidation: Insight into Pr dominance over Pt nanoparticles and metal–support interaction. *Appl. Catal. B Environ.* **2018**, *226*, 147–161. [CrossRef]
108. Sartoretti, E.; Martini, F.; Piumetti, M.; Bensaid, S.; Russo, N.; Fino, D. Nanostructured Equimolar Ceria-Praseodymia for Total Oxidations in Low-O_2 Conditions. *Catalysts* **2020**, *10*, 165. [CrossRef]
109. Mendiuk, O.; Nawrocki, M.; Kepinski, L. The synthesis of $Ce_{1-x}Ln_xO_{2-y}$ (Ln = Pr, Sm, Gd, Tb) nanocubes by hydrothermal methods. *Ceram. Int.* **2016**, *42*, 1998–2012. [CrossRef]
110. Hong, S.; Lee, D.; Yang, H.; Kim, Y.-B. Direct hydrothermal growth of GDC nanorods for low temperature solid oxide fuel cells. *Appl. Surf. Sci.* **2018**, *444*, 430–435. [CrossRef]
111. Yoshida, Y.; Fujihara, S. Shape-Controlled Synthesis and Luminescent Properties of CeO_2:Sm^{3+} Nanophosphors. *Eur. J. Inorg. Chem.* **2011**, *2011*, 1577–1583. [CrossRef]
112. Bhatta, U.M.; Reid, D.; Sakthivel, T.; Sayle, T.X.T.; Sayle, D.; Molinari, M.; Parker, S.C.; Ross, I.M.; Seal, S.; Möbus, G. Morphology and Surface Analysis of Pure and Doped Cuboidal Ceria Nanoparticles. *J. Phys. Chem. C* **2013**, *117*, 24561–24569. [CrossRef]
113. Ke, J.; Xiao, J.-W.; Zhu, W.; Liu, H.; Si, R.; Zhang, Y.-W.; Yan, C.-H. Dopant-Induced Modification of Active Site Structure and Surface Bonding Mode for High-Performance Nanocatalysts: CO Oxidation on Capping-free (110)-oriented CeO_2:Ln (Ln = La–Lu) Nanowires. *J. Am. Chem. Soc.* **2013**, *135*, 15191–15200. [CrossRef] [PubMed]
114. Xu, B.; Zhang, Q.; Yuan, S.; Zhang, M.; Ohno, T. Morphology control and photocatalytic characterization of yttrium-doped hedgehog-like CeO_2. *Appl. Catal. B Environ.* **2015**, *164*, 120–127. [CrossRef]
115. Małecka, M.A.; Kraszkiewicz, P.; Bezkrovnyi, O. Catalysis by shapely nanocrystals of the $Ce_{1-x}Yb_xO_{2-x/2}$ mixed oxides—Synthesis and phase stability. *Mater. Char.* **2019**, *155*, 109796. [CrossRef]
116. Roh, J.; Hwang, S.H.; Jang, J. Dual-Functional CeO_2:Eu^{3+} Nanocrystals for Performance-Enhanced Dye-Sensitized Solar Cells. *ACS Appl. Mater. Interfaces* **2014**, *6*, 19825–19832. [CrossRef]
117. Bo, Q.; Wang, J. Structural and optical properties of erbium doped ceria nanoparticles synthesized by hydrothermal method. *Spectrosc. Lett.* **2021**, *54*, 165–170. [CrossRef]
118. Yang, Y.; Cong, Y.; Dong, D.P.; Xiao, Y.; Shang, J.Y.; Tong, Y.; Zhang, H.M.; He, M.; Zhang, J.H. Structural and excitation dependent emission properties of octahedral CeO_2:Er^{3+} nanocrystal. *J. Lumin.* **2019**, *213*, 427–432. [CrossRef]
119. Wang, Z.L.; Feng, X. Polyhedral Shapes of CeO_2 Nanoparticles. *J. Phys. Chem. B* **2003**, *107*, 13563–13566. [CrossRef]
120. Yan, L.; Yu, R.; Chen, J.; Xing, X. Template-Free Hydrothermal Synthesis of CeO_2 Nano-octahedrons and Nanorods: Investigation of the Morphology Evolution. *Cryst. Growth Des.* **2008**, *8*, 1474–1477. [CrossRef]
121. Muñoz, F.F.; Acuña, L.M.; Albornoz, C.A.; Leyva, A.G.; Baker, R.T.; Fuentes, R.O. Redox properties of nanostructured lanthanide-doped ceria spheres prepared by microwave assisted hydrothermal homogeneous co-precipitation. *Nanoscale* **2015**, *7*, 271–281. [CrossRef]
122. Llusar, M.; Vitásková, L.; Šulcová, P.; Tena, M.A.; Badenes, J.A.; Monrós, G. Red ceramic pigments of terbium-doped ceria prepared through classical and non-conventional coprecipitation routes. *J. Eur. Ceram. Soc.* **2010**, *30*, 37–52. [CrossRef]
123. Acuña, L.M.; Muñoz, F.F.; Albornoz, C.A.; Leyva, A.G.; Baker, R.T.; Fuentes, R.O. Nanostructured terbium-doped ceria spheres: Effect of dopants on their physical and chemical properties under reducing and oxidizing conditions. *J. Mater. Chem. A* **2015**, *3*, 16120–16131. [CrossRef]
124. Xu, B.; Yang, H.; Zhang, Q.; Yuan, S.; Xie, A.; Zhang, M.; Ohno, T. Design and Synthesis of Sm, Y, La and Nd-doped CeO_2 with a broom-like hierarchical structure: A photocatalyst with enhanced oxidation performance. *ChemCatChem* **2020**, *12*, 2638–2646. [CrossRef]
125. Hirano, M.; Kato, E. Hydrothermal Synthesis of Nanocrystalline Cerium(IV) Oxide Powders. *J. Am. Ceram. Soc.* **1999**, *82*, 786–788. [CrossRef]
126. Basu, J.; Divakar, R.; Winterstein, J.P.; Carter, C.B. Low-temperature and ambient-pressure synthesis and shape evolution of nanocrystalline pure, La-doped and Gd-doped CeO_2. *Appl. Surf. Sci.* **2010**, *256*, 3772–3777. [CrossRef]
127. Polezhaeva, O.S.; Ivanov, V.K.; Dolgopolova, E.A.; Baranchikov, A.E.; Shcherbakov, A.B.; Tret'yakov, Y.D. Synthesis of Nanocrystalline Solid Solutions $Ce_{1-x}R_xO_2$-(R = Nd, Eu) by the Homogeneous Hydrolysis Method. *Dokl. Chem.* **2010**, *433*, 183–185. [CrossRef]
128. Dolgopolova, E.A.; Ivanova, O.S.; Ivanov, V.K.; Sharikov, F.Y.; Baranchikov, A.E.; Shcherbakov, A.B.; Trietyakov, Y.D. Microwave-hydrothermal synthesis of gadolinium-doped nanocrystalline ceria in the presence of hexamethylenetetramine. *Russ. J. Inorg. Chem.* **2012**, *57*, 1303–1307. [CrossRef]
129. Dunnick, K.M.; Pillai, R.; Pisane, K.L.; Stefaniak, A.B.; Sabolsky, E.M.; Leonard, S.S. The Effect of Cerium Oxide Nanoparticle Valence State on Reactive Oxygen Species and Toxicity. *Biol. Trace Elem. Res.* **2015**, *166*, 96–107. [CrossRef]

130. Dunnick, K.M.; Morris, A.M.; Badding, M.A.; Barger, M.; Stefaniak, A.B.; Sabolsky, E.M.; Leonard, S.S. Evaluation of the effect of valence state on cerium oxide nanoparticle toxicity following intratracheal instillation in rats. *Nanotoxicology* **2016**, *10*, 992–1000. [CrossRef]
131. Sato, K.; Arai, M.; Valmalette, J.-C.; Abe, H. Surface Capping-Assisted Hydrothermal Growth of Gadolinium-Doped CeO_2 Nanocrystals Dispersible in Aqueous Solutions. *Langmuir* **2014**, *30*, 12049–12056. [CrossRef] [PubMed]
132. Deng, T.; Zhang, C.; Xiao, Y.; Xie, A.; Pang, Y.U.E.; Yang, Y. One-step synthesis of samarium-doped ceria and its CO catalysis. *Bull. Mater. Sci.* **2015**, *38*, 1149–1154. [CrossRef]
133. Anantharaman, A.P.; Gadiyar, H.J.; Surendran, M.; Rao, A.S.; Dasari, H.P.; Dasari, H.; Babu, G.U.B. Effect of synthesis method on structural properties and soot oxidation activity of gadolinium-doped ceria. *Chem. Pap.* **2018**, *72*, 3179–3188. [CrossRef]
134. Yamamoto, K.; Hashishin, T.; Matsuda, M.; Qiu, N.; Tan, Z.; Ohara, S. High-performance Ni nanocomposite anode fabricated from Gd-doped ceria nanocubes for low-temperature solid-oxide fuel cells. *Nano Energy* **2014**, *6*, 103–108. [CrossRef]
135. Kempaiah, D.M.; Yin, S.; Sato, T. A facile and quick solvothermal synthesis of 3D microflower CeO_2 and Gd:CeO_2 under subcritical and supercritical conditions for catalytic applications. *CrystEngComm* **2011**, *13*, 741–746. [CrossRef]
136. Öksüzömer, M.A.F.; Dönmez, G.; Sariboğa, V.; Altinçekiç, T.G. Microstructure and ionic conductivity properties of gadolinia doped ceria ($Gd_xCe_{1-x}O_{2-x/2}$) electrolytes for intermediate temperature SOFCs prepared by the polyol method. *Ceram. Int.* **2013**, *39*, 7305–7315. [CrossRef]
137. Dönmez, G.; Sarıboğa, V.; Gürkaynak Altınçekiç, T.; Öksüzömer, M.A.F. Polyol Synthesis and Investigation of $Ce_{1-x}RE_xO_{2-x/2}$ (RE = Sm, Gd, Nd, La, $0 \leq x \leq 0.25$) Electrolytes for IT-SOFCs. *J. Am. Ceram. Soc.* **2015**, *98*, 501–509. [CrossRef]
138. Yang, Z.; Yin, Z.; Zhao, Z.; Yu, J.; Li, J.; Ren, Z.; Yu, G. Morphologies and magnetic properties of La-doped CeO_2 nanoparticles by the solvothermal method in a low magnetic field. *Mater. Chem. Phys.* **2020**, *240*, 122148. [CrossRef]
139. Thorat, A.V.; Ghoshal, T.; Carolan, P.; Holmes, J.D.; Morris, M.A. Defect Chemistry and Vacancy Concentration of Luminescent Europium Doped Ceria Nanoparticles by the Solvothermal Method. *J. Phys. Chem. C* **2014**, *118*, 10700–10710. [CrossRef]
140. Karaca, T.; Altınçekiç, T.G.; Faruk Öksüzömer, M. Synthesis of nanocrystalline samarium-doped CeO_2 (SDC) powders as a solid electrolyte by using a simple solvothermal route. *Ceram. Int.* **2010**, *36*, 1101–1107. [CrossRef]
141. Deepthi, N.H.; Darshan, G.P.; Basavaraj, R.B.; Prasad, B.D.; Nagabhushana, H. Large-scale controlled bio-inspired fabrication of 3D CeO_2:Eu^{3+} hierarchical structures for evaluation of highly sensitive visualization of latent fingerprints. *Sens. Actuators B Chem.* **2018**, *255*, 3127–3147. [CrossRef]
142. Godinho, M.; Gonçalves, R.d.F.; Leite, E.R.; Raubach, C.W.; Carreño, N.L.V.; Probst, L.F.D.; Longo, E.; Fajardo, H.V. Gadolinium-doped cerium oxide nanorods: Novel active catalysts for ethanol reforming. *J. Mater. Sci.* **2010**, *45*, 593–598. [CrossRef]
143. Prado-Gonjal, J.; Schmidt, R.; Espíndola-Canuto, J.; Ramos-Alvarez, P.; Morán, E. Increased ionic conductivity in microwave hydrothermally synthesized rare-earth doped ceria $Ce_{1-x}RE_xO_{2-(x/2)}$. *J. Power Source* **2012**, *209*, 163–171. [CrossRef]
144. Deus, R.C.; Cortés, J.A.; Ramirez, M.A.; Ponce, M.A.; Andres, J.; Rocha, L.S.R.; Longo, E.; Simões, A.Z. Photoluminescence properties of cerium oxide nanoparticles as a function of lanthanum content. *Mater. Res. Bull.* **2015**, *70*, 416–423. [CrossRef]
145. Silva, A.G.M.; Rodrigues, T.S.; Dias, A.; Fajardo, H.V.; Gonçalves, R.F.; Godinho, M.; Robles-Dutenhefner, P.A. $Ce_{1-x}Sm_xO_{1.9-\delta}$ nanoparticles obtained by microwave-assisted hydrothermal processing: An efficient application for catalytic oxidation of α-bisabolol. *Catal. Sci. Tech.* **2014**, *4*, 814–821. [CrossRef]
146. Bezkrovnyi, O.; Małecka, M.A.; Lisiecki, R.; Ostroushko, V.; Thomas, A.G.; Gorantla, S.; Kepinski, L. The effect of Eu doping on the growth, structure and red-ox activity of ceria nanocubes. *CrystEngComm* **2018**, *20*, 1698–1704. [CrossRef]
147. Slostowski, C.; Marre, S.; Bassat, J.-M.; Aymonier, C. Synthesis of cerium oxide-based nanostructures in near- and supercritical fluids. *J. Supercrit. Fluids* **2013**, *84*, 89–97. [CrossRef]
148. Xu, Y.; Farandos, N.; Rosa, M.; Zielke, P.; Esposito, V.; Vang Hendriksen, P.; Jensen, S.H.; Li, T.; Kelsall, G.; Kiebach, R. Continuous hydrothermal flow synthesis of Gd-doped CeO_2 (GDC) nanoparticles for inkjet printing of SOFC electrolytes. *Int. J. Appl. Ceram. Technol.* **2018**, *15*, 315–327. [CrossRef]
149. Karl Chinnu, M.; Vijai Anand, K.; Mohan Kumar, R.; Alagesan, T.; Jayavel, R. Synthesis and enhanced electrochemical properties of Sm:CeO_2 nanostructure by hydrothermal route. *Mater. Lett.* **2013**, *113*, 170–173. [CrossRef]
150. Dell'Agli, G.; Spiridigliozzi, L.; Marocco, A.; Accardo, G.; Ferone, C.; Cioffi, R. Effect of the Mineralizer Solution in the Hydrothermal Synthesis of Gadolinium-Doped (10% mol Gd) Ceria Nanopowders. *J. Appl. Biomater. Funct. Mater.* **2016**, *14*, 189–196. [CrossRef]
151. Wang, Z.; Wang, Q.; Liao, Y.; Shen, G.; Gong, X.; Han, N.; Liu, H.; Chen, Y. Comparative Study of CeO_2 and Doped CeO_2 with Tailored Oxygen Vacancies for CO Oxidation. *ChemPhysChem* **2011**, *12*, 2763–2770. [CrossRef]
152. Kim, G.; Lee, N.; Kim, K.-B.; Kim, B.-K.; Chang, H.; Song, S.-J.; Park, J.-Y. Various synthesis methods of aliovalent-doped ceria and their electrical properties for intermediate temperature solid oxide electrolytes. *Int. J. Hydrogen Energy* **2013**, *38*, 1571–1587. [CrossRef]
153. Sohn, Y. Lanthanide (III) (La, Pr, Nd, Sm, Eu, Gd, Tb, Dy, Ho, Er, Tm, and Yb) Ions Loaded in CeO_2 Support; Fundamental Natures, Hydrogen Reduction, and CO Oxidation Activities. *Appl. Sci. Converg. Technol.* **2019**, *28*, 35–40. [CrossRef]
154. Gnanam, S.; Gajendiran, J.; Ramana Ramya, J.; Ramachandran, K.; Gokul Raj, S. Glycine-assisted hydrothermal synthesis of pure and europium doped CeO_2 nanoparticles and their structural, optical, photoluminescence, photocatalytic and antibacterial properties. *Chem. Phys. Lett.* **2021**, *763*, 138217. [CrossRef]

155. Palard, M.; Balencie, J.; Maguer, A.; Hochepied, J.-F. Effect of hydrothermal ripening on the photoluminescence properties of pure and doped cerium oxide nanoparticles. *Mater. Chem. Phys.* **2010**, *120*, 79–88. [CrossRef]
156. Cabral, A.C.; Cavalcante, L.S.; Deus, R.C.; Longo, E.; Simões, A.Z.; Moura, F. Photoluminescence properties of praseodymium doped cerium oxide nanocrystals. *Ceram. Int.* **2014**, *40*, 4445–4453. [CrossRef]
157. Wang, P.; Kobiro, K. Synthetic versatility of nanoparticles: A new, rapid, one-pot, single-step synthetic approach to spherical mesoporous (metal) oxide nanoparticles using supercritical alcohols. *Pure Appl. Chem.* **2014**, *86*, 785–800. [CrossRef]
158. Xu, B.; Zhang, Q.; Yuan, S.; Liu, S.; Zhang, M.; Ohno, T. Synthesis and photocatalytic performance of yttrium-doped CeO_2 with a hollow sphere structure. *Catal. Today* **2017**, *281*, 135–143. [CrossRef]
159. Maria Magdalane, C.; Kaviyarasu, K.; Raja, A.; Arularasu, M.V.; Mola, G.T.; Isaev, A.B.; Al-Dhabi, N.A.; Arasu, M.V.; Jeyaraj, B.; Kennedy, J.; et al. Photocatalytic decomposition effect of erbium doped cerium oxide nanostructures driven by visible light irradiation: Investigation of cytotoxicity, antibacterial growth inhibition using catalyst. *J. Photochem. Photobiol. B* **2018**, *185*, 275–282. [CrossRef]
160. De Oliveira, R.C.; Cabral, L.; Cabral, A.C.; Almeida, P.B.; Tibaldi, N.; Sambrano, J.R.; Simões, A.Z.; Macchi, C.E.; Moura, F.; Marques, G.E.; et al. Charge transfer in Pr-Doped cerium oxide: Experimental and theoretical investigations. *Mater. Chem. Phys.* **2020**, *249*, 122967. [CrossRef]
161. Ren, Y.; Ma, J.; Ai, D.; Zan, Q.; Lin, X.; Deng, C. Fabrication and performance of Pr-doped CeO_2 nanorods-impregnated Sr-doped $LaMnO_3$–Y_2O_3-stabilized ZrO_2 composite cathodes for intermediate temperature solid oxide fuel cells. *J. Mater. Chem.* **2012**, *22*, 25042–25049. [CrossRef]
162. Jiang, Y.; Zou, L.; Cheng, J.; Huang, Y.; Wang, Z.; Chi, B.; Pu, J.; Li, J. Gadolinium doped ceria on graphene cathode with enhanced cycle stability for non-aqueous lithium-oxygen batteries. *J. Power Source* **2018**, *400*, 1–8. [CrossRef]
163. Shi, S.-J.; Zhou, S.-S.; Liu, S.-Q.; Chen, Z.-G. Photocatalytic activity of erbium-doped CeO_2 enhanced by reduced graphene Oxide/CuO cocatalyst for the reduction of CO_2 to methanol. *Environ. Prog. Sustain. Energy* **2018**, *37*, 655–662. [CrossRef]
164. Wang, Z.; Gu, F.; Wang, Z.; Han, D. Solvothermal synthesis of CeO_2:Er/Yb nanorods and upconversion luminescence characterization. *Mater. Res. Bull.* **2014**, *53*, 141–144. [CrossRef]
165. Aouissi, M.L.; Ghrib, A. Effect of Synthesis Route on Structural, Morphological Properties of $Ce_{0.8}Y_{0.2-x}La_xO_2$ (x = 0, 0.1, 0.2). *Bull. Chem. Soc. Jpn.* **2015**, *88*, 1159–1163. [CrossRef]
166. Zhao, R.; Huan, L.; Gu, P.; Guo, R.; Chen, M.; Diao, G. Yb,Er-doped CeO_2 nanotubes as an assistant layer for photoconversion-enhanced dye-sensitized solar cells. *J. Power Source* **2016**, *331*, 527–534. [CrossRef]
167. Han, D.; Yang, Y.; Gu, F.; Wang, Z. Tuning the morphology and upconversion fluorescence of CeO_2: Er/Yb nano-octahedra. *J. Alloys Compd.* **2016**, *656*, 524–529. [CrossRef]
168. Shirbhate, S.C.; Singh, K.; Acharya, S.A.; Yadav, A.K. Review on local structural properties of ceria-based electrolytes for IT-SOFC. *Ionics* **2017**, *23*, 1049–1057. [CrossRef]
169. Piumetti, M.; Andana, T.; Bensaid, S.; Fino, D.; Russo, N.; Pirone, R. Ceria-based nanomaterials as catalysts for CO oxidation and soot combustion: Effect of Zr-Pr doping and structural properties on the catalytic activity. *AIChE J.* **2017**, *63*, 216–225. [CrossRef]
170. Zhou, Y.; Deng, J.; Lan, L.; Wang, J.; Yuan, S.; Gong, M.; Chen, Y. Remarkably promoted low-temperature reducibility and thermal stability of CeO_2–ZrO_2–La_2O_3–Nd_2O_3 by a urea-assisted low-temperature (90 °C) hydrothermal procedure. *J. Mater. Sci.* **2017**, *52*, 5894–5907. [CrossRef]
171. Wang, C.; Wang, Y.; Huang, W.; Zou, B.; Khan, Z.S.; Zhao, Y.; Yang, J.; Cao, X. Influence of CeO_2 addition on crystal growth behavior of CeO_2–Y_2O_3–ZrO_2 solid solution. *Ceram. Int.* **2012**, *38*, 2087–2094. [CrossRef]
172. Khajavi, P.; Xu, Y.; Frandsen, H.L.; Chevalier, J.; Gremillard, L.; Kiebach, R.; Hendriksen, P.V. Tetragonal phase stability maps of ceria-yttria co-doped zirconia: From powders to sintered ceramics. *Ceram. Int.* **2020**, *46*, 9396–9405. [CrossRef]
173. Zhang, Y.; Zhang, L.; Deng, J.; Dai, H.; He, H. Controlled Synthesis, Characterization, and Morphology-Dependent Reducibility of Ceria−Zirconia−Yttria Solid Solutions with Nanorod-like, Microspherical, Microbowknot-like, and Micro-octahedral Shapes. *Inorg. Chem.* **2009**, *48*, 2181–2192. [PubMed]
174. Zhou, Y.; Xiong, L.; Deng, J.; Wang, J.; Yuan, S.; Lan, L.; Chen, Y. Facile synthesis of high surface area nanostructured ceria-zirconia-yttria-lanthana solid solutions with the assistance of lauric acid and dodecylamine. *Mater. Res. Bull.* **2018**, *99*, 281–291. [CrossRef]
175. Ozawa, M.; Yoshimura, Y.; Kobayashi, K. Structure and photoluminescence properties of $Ce_{0.5}Zr_{0.5}O_2$:Eu^{3+} nanoparticles synthesized by hydrothermal method. *Jpn. J. Appl. Phys.* **2017**, *56*, 01ae07. [CrossRef]
176. Ozawa, M.; Matsumoto, M.; Hattori, M. Photoemission properties of Eu-doped $Zr_{1-x}Ce_xO_2$ (x=0-0.2) nanoparticles prepared by hydrothermal method. *Jpn. J. Appl. Phys.* **2018**, *57*, 01ae04. [CrossRef]
177. Chen, H.; Shi, J.; Hua, Z.; Zhao, J.; Gao, J.; Lei, L.; Yan, D. Synthesis and Characteristics of La Doped Ceria–Zirconia Composite with Uniform Nano-Crystallite Dispersion. *Sci. Adv. Mater.* **2010**, *2*, 43–50.
178. Dudek, M. Ceramic Electrolytes in the CeO_2-Gd_2O_3-SrO System—Preparation, Properties and Application for Solid Oxide Fuel Cells. *Int. J. Electrochem. Sci.* **2012**, *7*, 2874–2889.
179. Dikmen, S. Effect of co-doping with Sm^{3+}, Bi^{3+}, La^{3+}, and Nd^{3+} on the electrochemical properties of hydrothermally prepared gadolinium-doped ceria ceramics. *J. Alloys Compd.* **2010**, *491*, 106–112. [CrossRef]

180. Dikmen, S.; Aslanbay, H.; Dikmen, E.; Şahin, O. Hydrothermal preparation and electrochemical properties of Gd^{3+} and Bi^{3+}, Sm^{3+}, La^{3+}, and Nd^{3+} codoped ceria-based electrolytes for intermediate temperature-solid oxide fuel cell. *J. Power Source* **2010**, *195*, 2488–2495. [CrossRef]
181. Hiley, C.I.; Walton, R.I. Controlling the crystallisation of oxide materials by solvothermal chemistry: Tuning composition, substitution and morphology of functional solids. *CrystEngComm* **2016**, *18*, 7656–7670. [CrossRef]
182. Minervini, L.; Zacate, M.O.; Grimes, R.W. Defect cluster formation in M_2O_3-doped CeO_2. *Solid State Ion.* **1999**, *116*, 339–349. [CrossRef]
183. Wang, J.D.; Xiao, X.; Liu, Y.; Pan, K.M.; Pang, H.; Wei, S.Z. The application of CeO_2-based materials in electrocatalysis. *J. Mater. Chem. A* **2019**, *7*, 17675–17702. [CrossRef]
184. Tyrsted, C.; Jensen, K.M.Ø.; Bøjesen, E.D.; Lock, N.; Christensen, M.; Billinge, S.J.L.; Iversen, B.B. Understanding the Formation and Evolution of Ceria Nanoparticles Under Hydrothermal Conditions. *Angew. Chem. Int. Ed.* **2012**, *51*, 9030–9033. [CrossRef]
185. Promethean Particles Products: Metal Oxides. Available online: https://prometheanparticles.co.uk/metal-oxides/ (accessed on 29 March 2021).
186. Wang, H.; Chen, X.; Gao, S.; Wu, Z.; Liu, Y.; Weng, X. Deactivation mechanism of Ce/TiO_2 selective catalytic reduction catalysts by the loading of sodium and calcium salts. *Catal. Sci. Tech.* **2013**, *3*, 715–722. [CrossRef]
187. Li, J.; Peng, Y.; Chang, H.; Li, X.; Crittenden, J.C.; Hao, J. Chemical poison and regeneration of SCR catalysts for NOx removal from stationary sources. *Front. Environ. Sci. Eng.* **2016**, *10*, 413–427. [CrossRef]
188. Kennedy, E.M.; Cant, N.W. Oxidative dehydrogenation of ethane and the coupling of methane over sodium containing cerium oxides. *Appl. Catal. A Gen.* **1992**, *87*, 171–183. [CrossRef]
189. Wright, C.S.; Walton, R.I.; Thompsett, D.; Fisher, J.; Ashbrook, S.E. One-step hydrothermal synthesis of nanocrystalline ceria-zirconia mixed oxides: The beneficial effect of sodium inclusion on redox properties. *Adv. Mater.* **2007**, *19*, 4500–4504. [CrossRef]
190. Soria, J.; Martinez-Arias, A.; Coronado, J.M.; Conesa, J.C. Chloride-induced modifications of the properties of rhodia/ceria catalysts. *Top. Catal.* **2000**, *11*, 205–212. [CrossRef]
191. Kępiński, L.; Okal, J. Occurrence and Mechanism of Formation of CeOCl in Pd/CeO_2 Catalysts. *J. Catal.* **2000**, *192*, 48–53. [CrossRef]
192. Spiridigliozzi, L.; Dell'Agli, G.; Biesuz, M.; Sglavo, V.M.; Pansini, M. Effect of the Precipitating Agent on the Synthesis and Sintering Behavior of 20 mol% Sm-Doped Ceria. *Adv. Mater. Sci. Eng.* **2016**, *2016*, 6096123. [CrossRef]
193. Mauro, M.; Crosera, M.; Monai, M.; Montini, T.; Fornasiero, P.; Bovenzi, M.; Adami, G.; Turco, G.; Filon, F.L. Cerium Oxide Nanoparticles Absorption through Intact and Damaged Human Skin. *Molecules* **2019**, *24*, 3759. [CrossRef] [PubMed]
194. Xu, Y.; Mofarah, S.S.; Mehmood, R.; Cazorla, C.; Koshy, P.; Sorrell, C.C. Design strategies for ceria nanomaterials: Untangling key mechanistic concepts. *Mater. Horiz.* **2021**, *8*, 102–123. [CrossRef]